Diploma Thesis

Influence of the CaO/SiO_2 on the early and long-term properties of alkali activated slag (AAS)

submitted in satisfaction of the requirements for the degree
Diplom-Ingenieur
of the TU Wien, Faculty of Civil and Environmental Engineering

---

Diplomarbeit

Einfluss des CaO/SiO_2 auf die Früh- und Langzeiteigenschaften von alkalisch aktivierter Schlacke (AAS)

ausgeführt zum Zwecke der Erlangung des akademischen Grads
Diplom-Ingenieur
eingereicht an der TU Wien, Fakultät für Bau- und Umweltingenieurwesen

Nikolaus Ebermann, BSc

Matr.Nr.: 01426333

Betreuung: Assistant Prof. **Teresa Liberto**, PhD
Shahid Muhammad, MSc
Univ.Prof.in **Agathe Robisson**, PhD
Institut für Werkstofftechnologie, Bauphysik und Bauökologie
Forschungsbereich Baustofflehre und Werkstofftechnologie
Technische Universität Wien
Karlsplatz 13/E207-01, 1040 Wien, Österreich

Wien, im Juni 2024

Acknowledgments

This thesis is a major milestone in my personal and academic life. After years of hard work, I would like to thank all the people who have helped and supported me along the way. I would especially like to thank my supervisors Prof. Teresa Liberto, PhD, Univ.Prof.in Agathe Robisson, PhD and Shahid Muhammad, MSc. Without their guidance, expertise, help and encouragement at every stage of the thesis, it would not have been possible.

I am also grateful to the entire team of E207-1: Research Unit of Building Materials for providing the academic environment and resources necessary for this study. In particular, I would like to thank Benjamin Marksteiner, who helped me to carry out the tests.

Special thanks to my boss and mentor Ing. Mag. Markus Neid for your understanding and flexibility during my studies. Your support in balancing my work and academic duties was crucial in allowing me to complete this thesis.

I would also like to acknowledge the support of my parents, Mag. Elisabeth and Mag. Christof Ebermann. They have always been very supportive and enabled me to pursue a career at the TU Wien. I would also like to thank my sister Stephanie Ebermann, BSc for her emotional support during my studies. A big thank you goes to my girlfriend Karoline Rosner, BSc who always supported me emotionally and believed in me.

I would like to thank my fellow students, who not only shared a similar journey, but also became friends. I am especially grateful for the help and friendship of Dr. Hainz Obermair, Dipl.-Ing. Alexander Urbas and Ing. Michael Reyes. Last but not least, I would also like to thank my friend Franziska Denkmayr, BA MA for her support during my studies and the writing of my thesis.

Kurzfassung

Eine nachhaltige Entwicklung unserer Gesellschaft wird immer wichtiger. Dies gilt auch für die Bauindustrie. Durch den Ersatz von gewöhnlichem Portlandzement (OPC) kann die Bauindustrie ihre CO_2-Emissionen erheblich reduzieren, da die Herstellung von OPC für 5-8% der gesamten anthropogenen CO_2-Emissionen verantwortlich ist. Ein vollständiger Ersatz kann durch alkalisch aktivierte Bindemittel (AAB) erreicht werden. AAB ist eine Mischung aus Alumosilikat haltigen Vorprodukten, die durch alkalische Aktivatoren aktiviert werden, die notwendig sind, um den Hydratationsprozess einzuleiten. In dieser Arbeit wird OPC vollständig durch alkalisch aktivierte Schlacke (AAS) ersetzt, eine Untergruppe der AAB, bei der Schlacke (GGBS) das Hauptvorprodukt ist. AAS kann die CO_2 Emissionen im Vergleich zu OPC um bis zu 20% reduzieren. Frühere Studien haben gezeigt, dass das optimale Kalzium Oxid zu Silizium Dioxid Verhältnis (CaO/SiO_2) von Schlacken variiert. Deshalb wird in dieser Studie eine Schlacke (Ecocem) ausgewählt und das CaO/SiO_2 durch den Einsatz von Zusatzstoffen geändert. Ecocem hat ein CaO/SiO_2 von 1.13 (Referenz). Kalzium Hydroxid ($Ca(OH)_2$) wird als Zusatzstoff verwendet, um das CaO/SiO_2 auf 1.50 zu erhöhen. Ludox, eine kolloidale Silizium (SiO_2) Lösung, wird verwendet, um das CaO/SiO_2 auf 0.80 und 0.50 zu reduzieren. Die früh- und langfristigen Eigenschaften dieser vier CaO/SiO_2 werden bei einem Wasser zu Feststoff Verhältnis (engl. *water to solid ratio*, w/s) von 0.66 untersucht. Das ist das kleinste w/s, bei dem alle vier verschiedenen CaO/SiO_2 verarbeitbar sind. Für $CaO/SiO_2 = 1.13$ wurde die AAS-Paste auch bei einem w/s = 0.50 getestet (ÖNORM EN 196-1 [33]).

Die AAS Pasten mit einem $CaO/SiO_2 = 1.50$ bei einem w/s = 0.66 zeigen eine sofortige Verringerung der Verarbeitbarkeit im Vergleich zur $CaO/SiO_2 = 1{,}13$. Dies ist auf die Zugabe von $Ca(OH)_2$, einem feinen Pulver, das den Wasserbedarf erhöht, zurückzuführen. Ebenso zeigen AAS Pasten mit einem niedrigeren CaO/SiO_2 von 0.80 und 0.50 bei einem w/s = 0.66 eine reduzierte Verarbeitbarkeit, die stärker ist, wenn mehr SiO_2 vorhanden ist. Auch hier ist Ludox eine fein verteilte Lösung mit hoher spezifischer Oberfläche und hohem Wasserbedarf. Die AAS Pasten mit einem $CaO/SiO_2 = 0.80$ erreichen am Tag 14 die besten mechanischen Eigenschaften.

Insgesamt ist zu erkennen, dass AAS Pasten mit mehr Kalziumgehalt ($CaO/SiO_2 = 1.13$ und 1.50) ein zementähnliches Verhalten in Bezug auf Hydratation und mechanische Eigenschaften aufweisen und von einer Lagerung unter Wasser profitieren. Die AAS Pasten mit weniger Kalziumgehalt ($CaO/SiO_2 = 0.50$ und 0.80) haben eine starke Verzögerung im Hydratationsprozess, die stärker wird, wenn mehr SiO_2 hinzugefügt wird. AAS Pasten mit $CaO/SiO_2 = 0.80$ erreichen nach anfänglicher Verzögerung gute mechanische Eigenschaften. Alle Daten weisen einen großen Fehlerbalken auf, was auf eine empfindliche Mischung hindeutet. Die AAS Pasten mit einem $CaO/SiO_2 = 0.50$ zeigen die schlechteste Hydratationsentwicklung und mechanische Eigenschaften. Durch diese systematische Studie wird deutlich, dass CaO/SiO_2 entscheidend für die früh- und langfristigen Eigenschaften von AAS ist.

Abstract

A sustainable development of our society is becoming increasingly important. This also applies to the construction industry. By replacing ordinary Portland cement (OPC), a strong impact on CO_2 reduction of the construction industry can be made. OPC production is indeed responsible for 5-8% of total anthropogenic CO_2 emissions. A complete replacement can be accomplished with alkali activated binders (AAB). AAB is a mixture of aluminosilicate precursors activated by alkali activators which are necessary to initiate the hydration process. In this thesis, a complete replacement of OPC was made with the use of alkali activated slag (AAS), a subcategory of AAB where the main precursor is slag (GGBS). AAS can reduce CO_2 emissions up to 20% compared to OPC. Some previous studies have shown that the optimum calcium oxide to silicon dioxide ratio (CaO/SiO_2) of slags varies. Therefore, in this study, a slag source (Ecocem) is selected and the CaO/SiO_2 is varied by using additives. Ecocem has a $CaO/SiO_2 = 1.13$ (reference). Calcium hydroxide ($Ca(OH)_2$) is used as an additive to increase the CaO/SiO_2 to 1.50. Ludox colloidal silica (SiO_2) suspension is used to reduce the CaO/SiO_2 to 0.80 and 0.50. The early and long term properties of these four CaO/SiO_2 are investigated at a water to solid ratio (w/s) = 0.66. This w/s is the one at which all the AAS pastes are workable. For $CaO/SiO_2 = 1.13$ the AAS paste was also tested at a w/s = 0.50 (ÖNORM EN 196-1[33]).

The AAS pastes with a $CaO/SiO_2 = 1.50$ at a w/s = 0.66, show an immediate reduction in workability compared to the $CaO/SiO_2 = 1.13$. This is due to the addition of $Ca(OH)_2$, a fine powder that increases the water demand. Similarly AAS pastes with a reduced CaO/SiO_2 to 0.80 and 0.50 with w/s = 0.66, show a reduced workability, stronger when more SiO_2 is present. Also here, Ludox is a nano dispersed solution with a high specific surface area and high water demand.

Overall, it can be seen that AAS pastes with more calcium content ($CaO/SiO_2 = 1.13$ and 1.50) have a more cement-like behavior in terms of hydration and mechanical properties and benefit from storage under water. The AAS pastes with a lower calcium content (CaO/SiO_2 = 0.50 and 0.80) have a severe delay in the hydration process, which is stronger when more SiO_2 is added. AAS pastes with $CaO/SiO_2 = 0.80$ achieve good mechanical properties after an initial delay. All data are characterized by a large error bar, suggesting a sensitive formulation. The AAS pastes with a $CaO/SiO_2 = 0.50$ have the worst hydration evolution and mechanical properties. With this systematic study, we demonstrate that CaO/SiO_2 plays a key role in the early and long-term properties of AAS.

Contents

Chapter 1

Introduction

A sustainable, environmentally friendly approach to development has become of increasingly importance in our world. Consequently, each industry must adapt and modify its common processes and materials in order to achieve more eco-friendly products. This is evident in the construction industry, where concrete remains one of the most commonly used materials. Concrete is a mixture of cement, aggregate, and water, with or without additional materials [6]. The environmental impact of concrete is a significant concern due to the CO_2 impact of cement used in its production [49].

This chapter addresses the environmental impact of cement, alternative materials to cement, prior studies on these alternatives, and their hydration process. At the end of the chapter, the motivation and research questions of this thesis will be presented.

1.1 Cement related emissions and sustainable alternatives

The term cement is generally used to refer to ordinary Portland cement (OPC). The production of OPC is responsible for 5-8% of the global CO_2 emissions [1, 13, 20, 57]. Furthermore, as presented in Figure 1.1, the production of cement has almost tripled from 1995 to 2021. In 2023, China was the largest producer of cement with a supply of 2100 million tons. The second largest producer of cement was India, with an output of 410 million tons. As these two countries are among the fastest growing in the world, it is likely that the increasing trend will continue [15, 52, 53]. The vast majority of CO_2 emissions are attributable to two distinct sources during cement

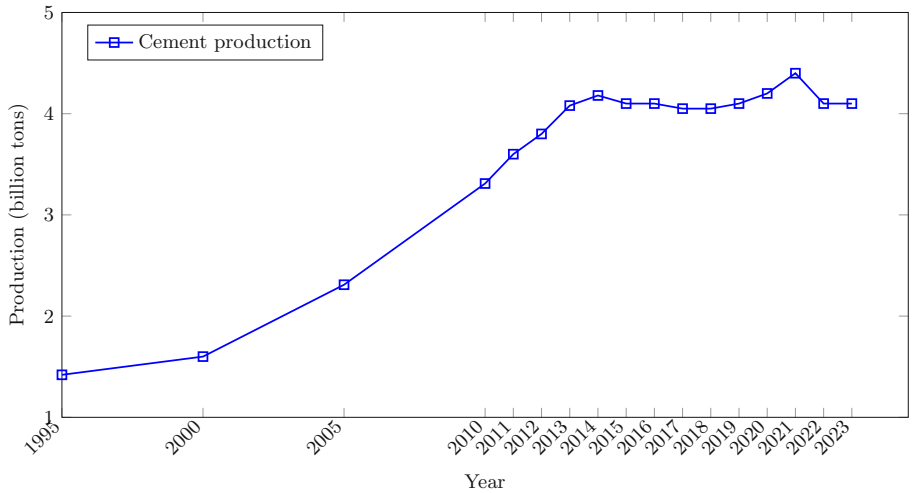

Fig. 1.1: Global cement production up to 2023 [53].

production:

- **heat production during sintering:** the production of cement consists in heating a mixture of limestone ($CaCO_3$) and clay in a rotary kiln at approximately 1450°C [5]. It relies heavily on the use of heat, predominantly derived from the combustion of fossil fuels. The product resulting from the combustion process is referred to as clinker. The addition of gypsum to the clinker results in the formation of OPC, the composition of which is detailed in Table 1.1. This process accounts for approximately 40% of CO_2 emissions related to cement [39, 51];

Tab. 1.1: Chemical composition of OPC [5].

CaO	SiO_2	Al_2O_3 + TiO_2	Fe_2O_3 (Fe)	Mn_2O_3 (MnO)	MgO	SO_3
64%	20%	5%	2.5%	0.1%	1.5%	2.5%

- **decomposition of limestone:** during sintering, limestone is decomposed into $CaCO_3 \longrightarrow CaO + CO_2$ [5, 51]. This process accounts for about 60% of CO_2 emissions production [39].

To reduce the CO_2 impact of construction industry, several alternatives to ordinary Portland cement have been developed. These include the common products from CEM II to CEM VI in accordance with recent 2021 ÖNORM EN 197-5 [37]. The clinker is partially replaced mainly by silica fume, pozzolana, fly ash, limestone and blast-furnace slag. The percentage of clinker is reduced to a total minimum of 5 to 19 percent in CEM III/C. The remaining material (81-95%) is blast furnace slag. Blast furnace slag and other aluminosilicate supplementary materials can be utilized as precursors of alkali activated binders (AAB), as described below [36, 51].

1.2 Alkali activated binder (AAB)

Alkali activated binders (AAB) offer an alternative to ordinary Portland cement (OPC) by completely replacing the clinker. AAB consists of an aluminosilicate precursor and an alkali activator [39]. The degree of CO_2 reduction depends on the used precursors, activators and their transport distance. A common precursor is blast furnace slag, a by-product of the steel-iron industry [40]. To replace OPC, this precursor must undergo an activation process. This involves mixing it with an alkaline activator to achieve a high pH [13]. The high pH is essential to initiate the chemical reactions necessary for the precursor to dissolve and then precipitate hydration products [21]. AAB can be classified in:

- **two-part AAB:** here the activator is an alkaline solution which is added to the precursors. As shown in Figure 1.2, the alkaline solutions are corrosive and therefore harmful [39]. Moreover, they generally have a high CO_2 emission [22, 39];

- **one-part AAB:** in comparison to the two-part ones, here the activator is an alkaline powder as shown in Figure 1.3. It is mixed with the precursor and water. This method is less harmful for workers and is more sustainable [22, 39].

Due to their faster hydration, two-parts AAB are more studied than one-part ones. The early age and long-term properties of AAB are significantly influenced by the type of precursor, the activator, and curing conditions [13]. Consequently, the workability of AAB, including aspects such as cohesiveness and pumpability, varies considerably. Due to these variations, they cannot be directly compared to OPC [21, 39]. This study will employ the one-part activation approach. The use of slag as precursors falls in the subcategory of alkali activated slag (AAS).

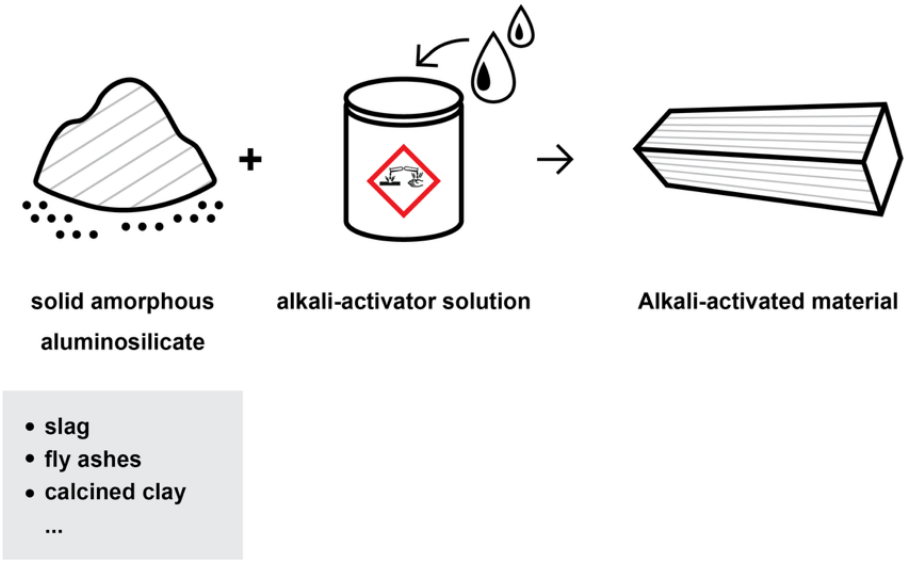

Fig. 1.2: Two-part AAB activation of a solid amorphous aluminosilicate [39].

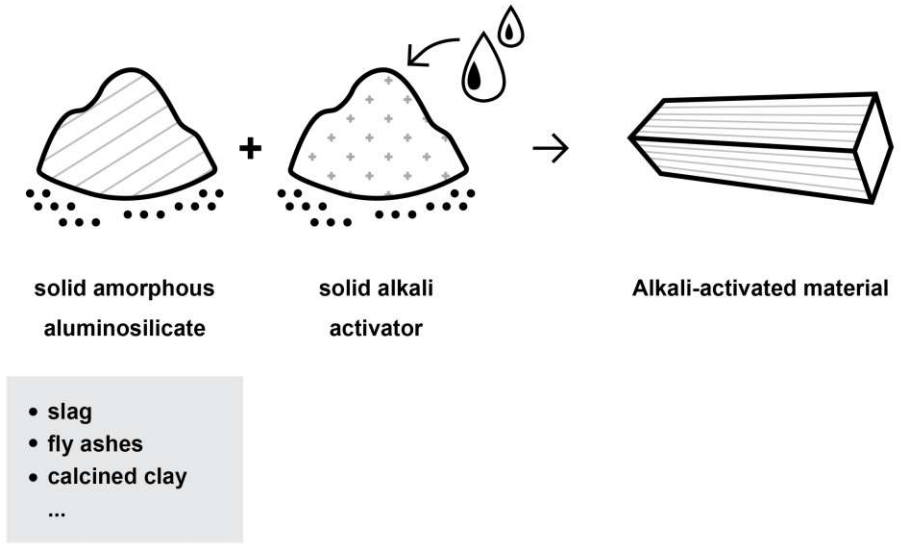

Fig. 1.3: One-part AAB activation of a solid amorphous aluminosilicate [39].

1.3 Alkali activated slag (AAS)

AAS has gained attention in the last decades due to its potential to completely replace traditional cement. In comparison to OPC, AAS can reduce CO_2 emissions up to 20 percent [12]. It is well known that the availability of slag will not increase in the future. However, a similar product can be made from white ladle steel slag [22], which is mostly landfilled today. A study by Garcia-Lodeiro et al. [13] has identified the essential properties of slags that are necessary for their use as precursors in alkali activated slag:

- the slag must be in granular or pellet form with a glass phase content greater than 85 - 95%;

- there should be a noticeable lack of structural order. A lower degree of polymerization in the glass increases its hydraulic activity, which is influenced by the arrangement of the (SiO_4) tetrahedra with Al and Mg in the glassy phase of the slag;
- the slag should have a basic pH, characterized by a $(CaO + MgO) / SiO_2$ ratio greater than one. This type of slag has greater hydraulic capacity due to its lime content, which facilitates activation. However, even acidic slags can undergo alkaline activation;
- grinding of the slag should produce a surface area between 400 - 600 m^2/kg. This specific surface measurement is critical as it directly affects the speed and strength of the activation process.

Thus, the typical chemical composition of slag, according to Garcia-Lodeiro et al. [13] are:

- 35 - 40% CaO calcium oxide
- 25 - 35% SiO_2 silicon dioxide
- 5 - 10% MgO magnesium oxide
- 5 - 15% Al_2O_3 aluminum oxide
- $<$ 1% S sulfur, Fe_2O_3 iron(III) oxide, MnO manganese(II) oxide and K_2O potassium oxide

As the content of SiO_2 and CaO is greater than 70%, AAS can be classified as a calcium and silicate rich material. Typically, slag is activated with sodium hydroxide (NaOH) and sodium silicate (Na_2SiO_3), which are referred to as two liquid solutions. Sodium carbonate (Na_2CO_3) an alkaline powder, is typically used in combination with the previous two [13, 22]. The alkali activation reaction mechanisms are described according to Garcia-Lodeiro et al. [13] as follows:

$$\equiv Si{-}O^- + R^+ \longrightarrow \equiv Si{-}O{-}R \tag{1.1}$$

$$\equiv Si{-}O{-}R + OH^- \longrightarrow \equiv Si{-}O{-}R{-}OH^- \tag{1.2}$$

$$\equiv Si{-}O{-}R{-}OH^- + Ca^{2+} \longrightarrow \equiv Si{-}O{-}Ca{-}OH + R^+ \tag{1.3}$$

The process initiates with an alkaline cation (R^+) reacting with a silicon-oxygen bond to form a new bond ($\equiv Si{-}O{-}R$), which serves as a catalyst. This is followed by the addition of a hydroxide ion (OH^-), which modifies the complex to ($Si{-}O{-}R{-}OH^-$). Subsequent to this, the complex interacts with calcium ions (Ca^{2+}), resulting in the formation of a calcium containing structure ($\equiv Si{-}O{-}Ca{-}OH + R^+$). Garcia-Lodeiro et al. [13] suggest that the alkaline cations (R^+) can be absorbed into the structure as the reactions progress. The anions (OH^-) present in the solution play a crucial role in the initial activation and the early age properties of the system. This process is shown in Figure 1.4 for one-part AAS. It is also valid for two-part AAS. The main reaction product of an alkali activated slag is C-A-S-H (calcium aluminum silicate hydrate) gel, which is structural analogous to the C-S-H (calcium silicate hydrate) gel formed by hydration of OPC despite the addition of aluminum [13, 22]. In accordance with Garcia-Lodeiro et al. [13], the following two points are commonly accepted in the field of alkali activated materials:

- C-A-S-H gel represents the primary hydration product. The gel formed from AAS exhibits a lower CaO/SiO_2 of 0.9-1.2 in comparison to C-S-H from OPC which is 1.7 to 2 [13, 23];
- the secondary products, as well as the amount of activators, slag structure, compositions and the curing conditions, have a significant impact on the structure and composition of the C-A-S-H gel.

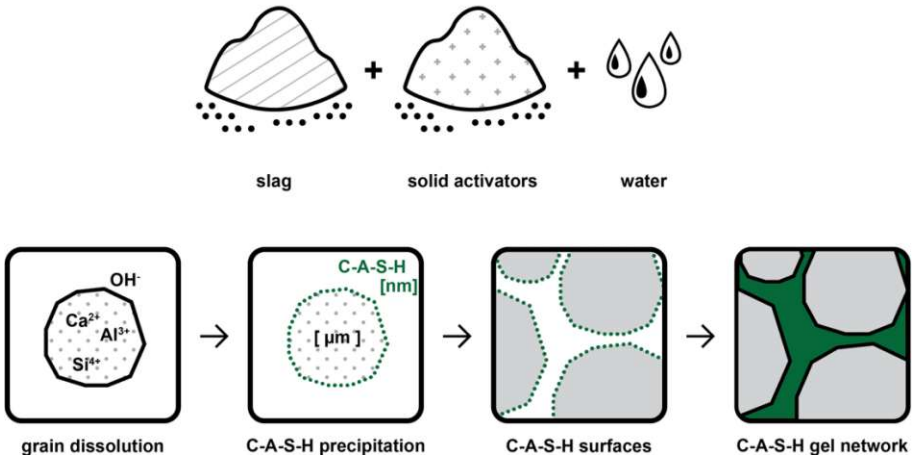

Fig. 1.4: One-part AAS reaction mechanism [39].

In this study, the one-part alkali activators of the GGBS (ground granulated blast-furnace slag) are sodium carbonate (Na_2CO_3) and calcium hydroxide ($Ca(OH)_2$), which have already been utilized in previous studies [21, 39]. The objective of this thesis is to study the role of CaO/SiO_2 on this specific one-part AAS formulation.

1.3.1 CaO/SiO_2 in cement

Considering the values of the chemical composition of an OPC powder from Table 1.1, a typical CaO/SiO_2 can be calculated as [5]:

$$CaO/SiO_2 = \frac{64}{20} = 3.20 \tag{1.4}$$

The addition of water to cement results in the formation of a C-S-H gel. The C-S-H gel has a typical CaO/SiO_2 of 1.7 to 2 after one hour of hydration [3, 23]. C-S-H has a variable stoichiometry and is generally expressed as [54]:

$$CaO : SiO_2 : H_2O \tag{1.5}$$

Beaudoin and Odler [3] have found that the CaO/SiO_2 of the powder decreases rapidly upon the formation of the C-S-H gel, from ~3.0 to 2.0-2.5. This is followed by a maximum value of 2.7-2.8. Thereafter, the ratio decreases again to values below 2. All this happens in the first hour of hydration. In addition to the water to solid ratio, the moment of measurement is also a crucial factor. With regard to the CaO/SiO_2, previous studies have identified the following points:

- the number of bridging Si tetrahedra decreases as the CaO/SiO_2 increases [23];
- in the context of low CaO/SiO_2, aluminum substitutes for silica in the bridging position [23];
- the elevated CaO/SiO_2 also results in a higher density. The density of cement is between 2.6 and 2.7 g/cm^3 [23];
- the CaO/SiO_2 reduces as the water to solid ratio (w/s) increases during the initial stages of the mixing process [3].

1.3.2 CaO/SiO_2 in slag

The typical CaO/SiO_2 for slag powder is usually less than 1.50. The exact ratio depends on the composition and dosage of the precursor [18]. The CaO/SiO_2 in the slag is comparable for different sources. However, the other components such as Al_2O_3, MgO, and TiO_2 of the slag can differ [11]. The alkali is used to activate the slag and also has an effect on the hydration products [13]. The dominant AAS hydration products are either calcium aluminosilicate hydrate (C-A-S-H) gels, or sodium containing calcium aluminosilicate silicate hydrate (C-(N-)A-S-H) gels [11]. The CaO/SiO_2 in the C-(N-)A-S-H gel is lower than the ratio of the powder, which is similar to the C-S-H gel in OPC [18]. The typical ratio is about $0.67 \leq CaO/SiO_2 \leq 1$, depending on the slag precursor and activators. For example C-(N-)A-S-H gel of slags activated with Na_2SiO_3 has a lower CaO/SiO_2 than that of those activated with NaOH because the first activator brings additional silica into the paste [18]. The gel of slags activated with Na_2CO_3 also has a lower CaO/SiO_2 because the Ca^{2+} cations are captured by the carbonate ions to precipitate calcite ($CaCO_3$) which is described in the following reaction:

$$CO_3{}^{2-} + Ca^{2+} \longrightarrow CaCO_3 \tag{1.6}$$

This reaction will happen before building C-A-S-H, which delays the hydration process [11].

A previous master thesis by Pudelko M. [39] shows how two different slag sources with different CaO/SiO_2 also present different mechanical properties. A $CaO/SiO_2 = 0.80$ seems to have a better early mechanical strength and to be sensitive to humidity variations compared to a $CaO/SiO_2 = 1.13$. The chemical composition of the two slags differs in the Al_2O_3 and MgO contents. This work needs a more systematic variation of CaO/SiO_2 to clarify the observed trend. The goal of this study is to vary the CaO/SiO_2 on the same slag source and analyze how the early and long term properties will change.

1.4 Methods

This section presents the theoretical framework and normative standards that apply to all of the tests conducted in this study.

1.4.1 Cone spread

The ÖNORM EN 12350-5 [31] outlines the standard cone spread test. This test involves lifting a standard sized Abrams cone and measuring the spread of a paste outside the cone as it flows out when the cone is lifted. Two diameters (d_1 and d_2) of the spread are measured. One is orthogonal to the other. The calculation of the average spread is as follows:

$$f = \frac{d_1 + d_2}{2} \tag{1.7}$$

The spread diameter allows the paste to be grouped in terms of consistency. They can be stiff plastic to very flowable [30]. The paste in the cone should always be lifted in the same way to ensure reproducibility. The surface should be slightly moist. From the spread, a value of dynamic yield stress (τ_y) (i.e., the stress needed to let the paste flow) can be calculated as follows [48]:

$$\tau_y = \frac{225 \cdot g \cdot \rho_{\text{total}} \cdot V^2}{128 \cdot \pi^2 \cdot r^5} \tag{1.8}$$

where:

τ_y is the dynamic yield stress in Pa $= 1 \times 10^{-6}$N/mm^2,
g is the acceleration due to gravity of 9.81 m/s^2,
ρ_{total} is the density of the mixture in kg/m^3,
V is volume of the cone in m^3,
r is half the spread diameter of the mixture calculated using Equation 1.8 in m.

1.4.2 Okamura

This method is used to optimize self-compacting concrete (SCC) mix designs. Okamura [27, 28] has developed a simple method to find the minimum ratio of water to solid, referred to as β_p. In other words, it determines whether all pores are filled with water. Achieving the correct ratio is essential for ensuring concrete homogeneity and workability. In order to determine the value of β_p, it is necessary to calculate the relative slump flow (see Equation 1.9) and the ratio of V_{water} and V_{solid}, which is usually between 1.1-1.4 [27, 28]. The relative slump flow Γ_m is calculated according to Okamura and Ouchi [29] as follows:

$$\Gamma_m = \left[\frac{((r_1 + r_2)/2)^2}{r_0}\right] - 1 \tag{1.9}$$

where:

Γ_m is the relative flow area normally between 1-4 [-],
r_1 is the halve of the first measured spread diameter in m,
r_2 is the halve of the second measured spread diameter in m,
r_o is the halve of the base diameter of the cone in m.

β_p is obtained by a linear trend line through the results of four different volumes of w/s and corresponding relative slump flows.

1.4.3 Vicat

In order to determine the initial and final setting point of a hydrating paste, the vicat test is employed. The initial setting point can be defined as the point when the paste begins to lose its workability. The final setting time is the time when the workability is lost and the mechanical properties begin to increase [54, 56]. For OPC, the initial setting time is one hour at the earliest and the final setting time is 12 hours at the latest [5]. Those two points in time are obtained through a needle penetration test (vicat) in accordance with the ÖNORM EN 196-3 [35]. The norm defines three penetration depths obtained with a needle on paste filled in a cone (h= 40 mm). The initial setting time is defined at a needle penetration depth of 37.0 - 31.0 mm. The final setting time is when the penetration depth of the needle reaches less than 0.50 mm.

The time when the penetration depth reaches 37, 31, and 0.5 mm is determined by linear interpolation. The linear interpolation is calculated as follows for an example of 37 mm:

$$t = t_1 + \left(\frac{37 - y_1}{y_2 - y_1}\right)(t_2 - t_1) \tag{1.10}$$

where:

y_1 is the penetration depth value that is greater than 37 mm and has the smallest gap,
t_1 is the time that belongs to y_1,
y_2 is the penetration depth value that is lower than 37 mm and has the smallest gap,
t_2 is the time that belongs to y_2,
t is the designated time at which the specified penetration depth of 37mm is reached.

Several vicat tests were performed with the same time interval between each penetration depth. The error bar is calculated as follows (for each of the three penetration depths):

$$\sigma_t = \frac{|t_2 - t_1|}{|y_2 - y_1|}\sqrt{\sigma_{y1}^2 + \sigma_{y2}^2} \tag{1.11}$$

where:

σ_{y1} is the standard deviation of y_1,
σ_{y2} is the standard deviation of y_2.

The precise methodology employed in the test will be detailed in Subsection 2.2.3.

1.4.4 Isothermal calorimetry

Isothermal calorimetry is commonly used to measure the heat of hydration of cement and other binders over time. The hardening process of reactive binder is an exothermic process [54], which means that heat is released when the powder comes into contact with a solution. The evolution of the heat of hydration can be measured in an isothermal calorimeter, in Joule per gram (J/g) and is linked to formation of hydration products over time. The hydration process, from contact with water towards setting, affects the workability of pastes [54]. The heat of hydration of the paste is calculated by comparing it to a reference. According to ÖNORM EN 196-11 [34], the mass of the reference, for instance sand, is calculated as follows:

$$m_{\text{sand}}^{\text{reference}} = \frac{C_{\text{total}}}{c_{\text{sand}}^{\text{reference}}} = \frac{\sum_{i=1}^{n} m_{\text{i}}^{\text{paste}} \cdot c_{\text{i}}^{\text{paste}}}{c_{\text{sand}}^{\text{reference}}} \tag{1.12}$$

where:

$m_{\text{sand}}^{\text{reference}}$ is mass of the reference,
C_{total} is the heat capacity of the total paste in $\text{J} \cdot \text{K}^{-1}$,
$m_{\text{i}}^{\text{paste}}$ is of each ingredients of the paste in g,
$c_{\text{i}}^{\text{paste}}$ is the specific heat capacity of each ingredients of the paste in $\text{J} \cdot \text{g}^{-1} \cdot \text{K}^{-1}$,
$c_{\text{sand}}^{\text{reference}}$ is the specific heat capacity of the reference in $\text{J} \cdot \text{g}^{-1} \cdot \text{K}^{-1}$.

1.4.5 Mortar prism

Once the final setting point is reached, the paste loses its workability and we have a solid product. In order to measure the flexural and compressive strength of the hardened pastes, the ÖNORM EN 196-1 [33] contains a standard method for the preparation and testing of mortar prisms. The latter are obtained by mixing the fresh paste with standard sand, typically in a ratio of 1:3 by weight. The particle size distribution in standard sand is shown in Table 1.2. For

Tab. 1.2: Distribution of particle sizes of norm sand [33].

Mesh size mm	2.0-1.6	1.6-1.0	1.0-0.5	0.5-0.16	0.16-0.08
Percentage %	8	26	34	20	12

the measurement of the flexural and compressive strength the ÖNORM EN 196-1 [33] presents the following two equations. The flexural strength R_f is calculated in megapascal as shown in Equation 1.13 according to ÖNORM EN 196-1 [33]:

$$R_f = \frac{1.5 \cdot F_f \cdot l}{b^3} \tag{1.13}$$

where:

R_f is the flexural strength in MPa = N/mm^2,
b is the side of the square sections of the prism in mm,
F_f is the load applied to the middle of the prism at fracture in N,
l is the distance between the supports in mm.

The compressive strength R_c is calculated in megapascal as shown in Equation 1.14 according to ÖNORM EN 196-1 [33]:

$$R_c = \frac{F_c}{A} \tag{1.14}$$

where:

R_c is the compressive strength in MPa = N/mm^2,
F_c is the maximum load at fracture in N,
A is the square section's area.

According to the Prüfverfahren Beton (PVB) [38] guidelines, the maximum stress limit should be reached within a 30 to 60 second time frame, as if the stress limit is reached too rapidly, the outcomes may be erroneous.

1.5 Motivation and research question

Pudelko M. [39] has shown that different mechanical properties are obtained for slag sources with different CaO/SiO_2. In the literature, the influence of CaO/SiO_2 on the early and long term properties of alkali activated slag is not clear and not extensively studied for the formulation used in this thesis. Wang et al. [55] showed that the best CaO/SiO_2 for AAS pastes is 1.00. However, Luo and Wang [24] mentioned the optimum CaO/SiO_2 for AAS pastes is 0.42. They both used a

different slag precursor. This thesis analyze how the CaO/SiO_2 influences the properties of alkali activated slag on the same slag source (i.e., GGBS). **In this study the CaO/SiO_2 is varied by using additives, as detailed in the next chapter to define how the CaO/SiO_2 in AAS formulations affects their early and long term properties.**

Chapter 2

Materials and methods

The following chapter provides a detailed description of the materials and the methodologies used in this thesis.

2.1 Materials

The main material studied in this thesis is an alkali activated slag (AAS), which consists of:

- precursor: ground and granulated blast-furnace slag (GGBFS) from Ecocem;
- activators: sodium carbonate Na_2CO_3 and calcium hydroxide $Ca(OH)_2$.

This Ecocem GGBS has a CaO/SiO_2 of 1.13. Pudelko M. [39] showed that a GGBS with a CaO/SiO_2 of 0.80 has good initial strength values that decrease over time. To investigate the role of CaO/SiO_2 without changing the other components of GGBS, two additives were used:

- Ludox® TM-50 colloidal silica SiO_2 suspension;
- $Ca(OH)_2$.

These main materials listed above will be described in more detail in the next subsections.

2.1.1 Ground and granulated blast-furnace slag (GGBS)

As mentioned in Section 1.3, slag, or more specifically ground granulated blast-furnace slag can be used as a precursor for the production of AAS. In this study, the GGBS is sourced from Ecocem France SAS [10]. The density of this is material $\rho = 2.94$ g/cm^3 and the median of the particle size distribution is $D_{50} = 11.0$ μm [39]. The chemical composition of Ecocem GGBS is shown in Table 2.1. Ecocem has a weight percent of 35.70% SiO_2 (silicon dioxide) and

Tab. 2.1: Chemical composition of Ecocem [39].

Oxide	SiO_2	CaO	Al_2O_3	Fe_2O_3	MgO	SO_3	MnO	K_2O	Na_2O	TiO_2	P_2O_5
wt%	35.7	40.4	12.1	1.5	6.5	1.9	0.4	0.5	0.3	0.9	<0.1

40.40% CaO (calcium oxide), which are its main two constituents. This results in a calcium oxide to silicon dioxide ratio, of:

$$CaO/SiO_2 = 1.13 \tag{2.1}$$

2.1.2 Solid activators

To obtain AAS from GGBS, it is necessary to add two solid activators to the slag:

- sodium carbonate Na_2CO_3;
- calcium hydroxide $Ca(OH)_2$.

Both are produced by Chem-Lab NV [7]. The densities and the molecular weights of the two activators are shown in Table 2.2. These solid activators were chosen in accordance with previous

Tab. 2.2: Properties of activators.

Name	Chem. formula	Density (ρ)	Molecular weight (MW)	Role
Sodium carbonate	Na_2CO_3	2.53 g/cm^3	105.99 g/mol	Activator
Calcium hydroxide	$Ca(OH)_2$	2.24 g/cm^3	74.10 g/mol	Activator/ Additive
Ludox	SiO_2	1.40 g/cm^3	60.08 g/mol	Additive

works [21, 22]. These previous studies have identified an optimized formulation for alkali activated slag (AAS). The percentages of activators used are fixed: 5.0 % Na_2CO_3 and 3.5 % $Ca(OH)_2$ (see Figure 2.1). This mixture makes use of stoichiometric amounts of Na_2CO_3 and $Ca(OH)_2$. This formulation provides good mechanical properties both initially and over time, while maintaining a low CO_2 impact. The two activators Na_2CO_3 and $Ca(OH)_2$ once in contact with water react

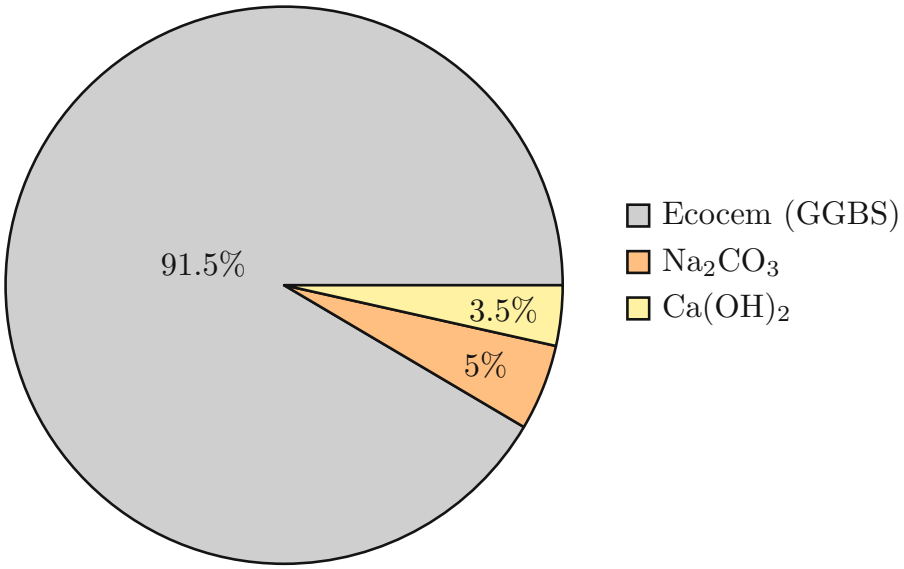

Fig. 2.1: The alkali activated slag's (AAS) composition [39].

to form sodium hydroxide NaOH and calcite $CaCO_3$:

$$Na_2CO_3 + Ca(OH)_2 \longrightarrow 2\,NaOH + CaCO_3. \tag{2.2}$$

Sodium hydroxide (NaOH) is well known to be highly alkaline. Once NaOH is formed, GGBS begins to dissolve and the hydration process begins [11]. The amount of activator is kept constant for all formulations used in the thesis and is not taken into account in the calculation of CaO/SiO_2.

2.1.3 Additives

In order to change the CaO/SiO_2 of Ecocem two different additives have been used in this study. The first additive that has been used to decrease the CaO/SiO_2 is Ludox®TM-50 colloidal silica (SiO_2) from Sigma Aldrich [8] which is in a 50 wt% suspension in H_2O, from now on called Ludox. The second additive used to increase the CaO/SiO_2 of the paste is calcium hydroxide $Ca(OH)_2$ which is the same material used as an activator. However, as already highlighted, only the amount which is used as an additive is taken into account for the calculation of the CaO/SiO_2. The density (ρ) and the molecular weight (MW) of the two additives are reported in Table 2.2. As already mentioned, they are both used to change the CaO/SiO_2:

- **ludox** was used to decrease the CaO/SiO_2 to 0.50 and 0.80;
- **calcium hydroxide** was used to increase the CaO/SiO_2 to 1.50.

2.1.4 Formulations

A total of four CaO/SiO_2 were studied in this thesis:

- 0.50
- 0.80
- 1.13 (Reference)
- 1.50

Considering the contribution of the original GGBS (i.e., CaO^{eco}, ${SiO_2}^{eco}$) and that of the additives present (i.e., CaO^{add}, ${SiO_2}^{add}$):

$$\frac{CaO}{SiO_2} = \frac{CaO^{eco} + CaO^{add}}{{SiO_2}^{eco} + {SiO_2}^{add}} \tag{2.3}$$

The calculation of the quantity of each component in each formulation is detailed below. The total volume, V_T is calculated as follows (with act standing for activators):

$$V_T = V_{eco} + V_{act} + V_{add} + V_{water} \tag{2.4}$$

$$V_T = \frac{m_{eco}}{\rho_{eco}} + \frac{m^{act}_{Na_2CO_3}}{\rho_{Na_2CO_3}} + \frac{m^{act}_{Ca(OH)_2}}{\rho_{Ca(OH)_2}} + \frac{m_{add}}{\rho_{add}} + \frac{m_{water}}{\rho_{water}} \tag{2.5}$$

The water to solid ratio is calculated as follows:

$$\frac{water}{solid} = \frac{w}{s} = \frac{m_{water}}{m_{eco} + m^{act}_{Na_2CO_3} + m^{act}_{Ca(OH)_2} + m^{add}} \tag{2.6}$$

As discussed in Section 2.1.3, the GGBS is activated by specific ratio of 5.0% sodium carbonate and 3.5% calcium hydroxide [21] (see Figure 2.1). The alkali activated slag (AAS) will always consist out of:

- 91.5% Ecocem
- 5.0% Na_2CO_3
- 3.5% $Ca(OH)_2$

As the ratio of slag and the two activators is always the same, the mass of activators can be expressed through the mass of Ecocem:

$$m^{act}_{Na_2CO_3} = \frac{5.0}{91.5} \cdot m_{eco} \tag{2.7}$$

$$m^{act}_{Ca(OH)_2} = \frac{3.5}{91.5} \cdot m_{eco} \tag{2.8}$$

If Equations 2.7 and 2.8 are inserted into Equations 2.5, Equations 2.9 respectively 2.10 are obtained.

$$V_T = \frac{m_{eco}}{\rho_{eco}} + \frac{\frac{5.0}{91.5} \cdot m_{eco}}{\rho^{act}_{Na_2CO_3}} + \frac{\frac{3.5}{91.5} \cdot m_{eco}}{\rho^{act}_{Ca(OH)_2}} + \frac{m_{water}}{\rho_{water}} \tag{2.9}$$

$$V_T = \frac{m_{eco}}{\rho_{eco}} + \frac{\frac{5.0}{91.5} \cdot m_{eco}}{\rho^{act}_{Na_2CO_3}} + \frac{\frac{3.5}{91.5} \cdot m_{eco}}{\rho^{act}_{Ca(OH)_2}} + \frac{m_{add}}{\rho_{add}} + \frac{m_{water}}{\rho_{water}} \tag{2.10}$$

The subsequent step involves determining the appropriate m_{add} and m_{water} in relation to the mass of Ecocem. The additive Ludox is added in a water solution, while the additive $Ca(OH)_2$ is added as a solid component together with Ecocem. This requires precise calculations of different w/s ratios for each additive and for the reference where no additive is taken into account. Therefore, an example for each option is provided below.

2.1.4.1 Calculation for the reference formulation (CaO/SiO_2 = 1.13)

The mass of water is calculated by inserting Equations 2.7 and 2.8 into Equation 2.6 obtaining:

$$m_{water} = \frac{100}{91.5} \cdot w/s \cdot m_{eco} \tag{2.11}$$

The total volume is then calculated as follows:

$$V_T = \frac{m_{eco}}{\rho_{eco}} + \frac{\frac{5.0}{91.5} \cdot m_{eco}}{\rho^{act}_{Na_2CO_3}} + \frac{\frac{3.5}{91.5} \cdot m_{eco}}{\rho^{act}_{Ca(OH)_2}} + \frac{\frac{100.0}{91.5} \cdot w/s \cdot m_{eco}}{\rho_{water}} \tag{2.12}$$

The calculation of the mass of the Ecocem will then be carried out as follows:

$$m_{eco} = \frac{V}{\frac{1}{\rho_{eco}} + \frac{\frac{5.0}{91.5}}{\rho^{act}_{Na_2CO_3}} + \frac{\frac{3.5}{91.5}}{\rho^{act}_{Ca(OH)_2}} + \frac{\frac{100.0}{91.5} \cdot w/s}{\rho_{water}}} \tag{2.13}$$

2.1.4.2 Calculation for the formulation containing Ludox (CaO/SiO_2 = 0.50 and 0.80)

This subsection will examine the calculations required to reduce the CaO/SiO_2 by using Ludox. Ludox, as already discussed in Section 2.1.3, is a 50 wt. % suspension in H_2O. Accordingly, the mass of the Ludox is 50% water (H_2O) and 50% solid Ludox (SiO_2):

$$m^{add}_{\text{Ludox, total}} = 0.5 \cdot m^{add}_{\text{Ludox, solid}} + 0.5 \cdot m^{add}_{\text{Ludox, water}} \tag{2.14}$$

The desired ratio of CaO/SiO_2 can be calculated in the following way:

$$\frac{CaO}{SiO_2} = \frac{CaO^{eco}}{SiO_2{}^{eco} + \frac{m^{add}_{\text{Ludox, total}}}{2}} \tag{2.15}$$

Substituting CaO^{eco}, $SiO_2{}^{eco}$ (see Table 2.1), we obtain:

$$\frac{CaO}{SiO_2} = \frac{m_{eco} \cdot 0.404}{m_{eco} \cdot 0.357 + \frac{m^{add}_{Ludox,\ total}}{2}} \tag{2.16}$$

The total mass of ludox will then be the result of Equation 2.17:

$$m^{add}_{Ludox,\ total} = \frac{(m_{eco} \cdot 0.404 - CaO/SiO_2 \cdot m_{eco} \cdot 0.357) \cdot 2}{CaO/SiO_2} \tag{2.17}$$

The w/s is then calculated as follows:

$$w/s = \frac{m^{add}_{Ludox,\ water} + m_{water,\ added}}{m_{eco} + m^{act}_{Na_2CO_3} + m^{act}_{Ca(OH)_2} + m^{add}_{Ludox,\ solid}} \tag{2.18}$$

Then the mass of added water is calculated in the following way:

$$m_{water,\ added} = w/s \cdot \left(m_{eco} + m^{act}_{Na_2CO_3} + m^{act}_{Ca(OH)_2} + m^{add}_{Ludox,\ solid}\right) - m^{add}_{Ludox,\ water} \tag{2.19}$$

The total volume can be calculated as follows:

$$\begin{aligned} V_T = {} & \frac{m_{eco}}{\rho_{eco}} + \frac{\frac{5.0}{91.5} \cdot m_{eco}}{\rho^{act}_{Na_2CO_3}} + \frac{\frac{3.5}{91.5} \cdot m_{eco}}{\rho^{act}_{Ca(OH)_2}} + \frac{\frac{(m_{eco} \cdot 0.404 - CaO/SiO_2 \cdot m_{eco} \cdot 0.357) \cdot 2}{CaO/SiO_2} \cdot m_{eco}}{\rho^{add}_{Ludox}} \\ & + \frac{w/s \cdot \left(m_{eco} + \frac{5.0}{91.5} \cdot m_{eco} + \frac{3.5}{91.5} \cdot m_{eco}\right)}{\rho_{water}} + \frac{w/s \cdot 0.5 \cdot \frac{(m_{eco} \cdot 0.404 - CaO/SiO_2 \cdot m_{eco} \cdot 0.357) \cdot 2}{CaO/SiO_2} \cdot m_{eco}}{\rho_{water}} \\ & - \frac{0.5 \cdot \frac{(m_{eco} \cdot 0.404 - CaO/SiO_2 \cdot m_{eco} \cdot 0.357) \cdot 2}{CaO/SiO_2} \cdot m_{eco}}{\rho_{water}} \end{aligned} \tag{2.20}$$

The calculation of the mass of the Ecocem will then be carried out as follows:

$$\begin{aligned} m_{eco} = {} & \frac{V}{\frac{1}{\rho_{eco}} + \frac{\frac{5.0}{91.5}}{\rho^{act}_{Na_2CO_3}} + \frac{\frac{3.5}{91.5}}{\rho^{act}_{Ca(OH)_2}} + \frac{\frac{(0.404 - CaO/SiO_2 \cdot 0.357) \cdot 2}{CaO/SiO_2}}{\rho^{add}_{Ludox}}} \\ & + \frac{V}{\frac{w/s \cdot \left(1 + \frac{5.0}{91.5} + \frac{3.5}{91.5}\right)}{\rho_{water}} + \frac{w/s \cdot 0.5 \cdot \frac{(0.404 - CaO/SiO_2 \cdot 0.357) \cdot 2}{CaO/SiO_2}}{\rho_{water}} - \frac{0.5 \cdot \frac{(0.404 - CaO/SiO_2 \cdot 0.357) \cdot 2}{CaO/SiO_2}}{\rho_{water}}} \end{aligned} \tag{2.21}$$

2.1.4.3 Calculation for the formulation containing $Ca(OH)_2$ ($CaO/SiO_2 = 1.50$)

To calculate the amount of $Ca(OH)_2$ as an additive, we use the following equation:

$$\frac{CaO}{SiO_2} = \frac{CaO^{eco} + CaO^{add}}{SiO_2{}^{eco}} \tag{2.22}$$

As in Subsection 2.1.4.2, the information from Table 2.1 can be inserted and Equation 2.22 can be reformulated as follows:

$$\frac{CaO}{SiO_2} = \frac{m_{eco} \cdot 0.404 + m_{CaO}}{m_{eco} \cdot 0.357} \tag{2.23}$$

The mass of CaO can then be calculated as presented in the following Equation 2.24:

$$m_{\mathrm{CaO}} = (0.357 \cdot \mathrm{CaO/SiO_2} - 0.404) \cdot m_{\mathrm{eco}} \tag{2.24}$$

Equation 2.22 uses a ratio of CaO to SiO_2 and not a ratio of $Ca(OH)_2$ to SiO_2. Therefore, it is necessary to determine the molecular weights of CaO and $Ca(OH)_2$. The molecular mass of $Ca(OH)_2$ and CaO can then be calculated as follows:

$$\mathrm{MW_{Ca(OH)_2}} = \mathrm{MW_{Ca}} + 2 \cdot (\mathrm{MW_O} + \mathrm{MW_H}) = 40.08 + 2 \cdot (16 + 1) = 74.08\,\mathrm{g/mol} \tag{2.25}$$

$$\mathrm{MW_{CaO}} = \mathrm{MW_{Ca}} + \mathrm{MW_O} = 40.08 + 16 = 56.08\,\mathrm{g/mol} \tag{2.26}$$

Next, the mass of $Ca(OH)_2$ is calculated by the ratio of the molecular masses and as a function of the mass of CaO as follows:

$$m^{add}_{\mathrm{Ca(OH)_2}} = \frac{m^{\mathrm{added}}_{\mathrm{CaO}} \cdot \mathrm{MW_{Ca(OH)_2}}}{\mathrm{MW_{CaO}}} \tag{2.27}$$

The desired ratio of CaO/SiO_2 can be calculated in the following way:

$$m^{add}_{\mathrm{Ca(OH)_2}} = \frac{(0.357 \cdot \mathrm{CaO/SiO_2} - 0.404) \cdot 74.08\,\mathrm{g/mol} \cdot m_{\mathrm{eco}}}{56.08\,\mathrm{g/mol}} \tag{2.28}$$

The w/s is then calculated as follows:

$$w/s = \frac{m_{\mathrm{water}}}{m_{\mathrm{eco}} + m^{act}_{\mathrm{Na_2CO_3}} + m^{act}_{\mathrm{Ca(OH)_2}} + m^{add}_{\mathrm{Ca(OH)_2}}} \tag{2.29}$$

The mass of added water is calculated as:

$$m_{\mathrm{water}} = w/s \cdot \left(m_{\mathrm{eco}} + m^{\mathrm{act}}_{\mathrm{Na_2CO_3}} + m^{\mathrm{act}}_{\mathrm{Ca(OH)_2}} + m^{\mathrm{add}}_{\mathrm{Ca(OH)_2}}\right) \tag{2.30}$$

The total volume is calculated by inserting all the Equations in this subsection into Equation 2.5 obtaining:

$$\begin{aligned} V_{\mathrm{T}} = {} & \frac{m_{\mathrm{eco}}}{\rho_{\mathrm{eco}}} + \frac{\frac{5.0}{91.5} \cdot m_{\mathrm{eco}}}{\rho^{\mathrm{act}}_{\mathrm{Na_2CO_3}}} + \frac{\frac{3.5}{91.5} \cdot m_{\mathrm{eco}}}{\rho^{\mathrm{act}}_{\mathrm{Ca(OH)_2}}} + \frac{\frac{(0.357 \cdot \mathrm{CaO/SiO_2} - 0.404) \cdot 74.08\,\mathrm{g/mol} \cdot m_{\mathrm{eco}}}{56.08\,\mathrm{g/mol}}}{\rho^{\mathrm{add}}_{\mathrm{Ca(OH)_2}}} \\ & + \frac{w/s \cdot \left(m_{\mathrm{eco}} + \frac{5.0}{91.5} \cdot m_{\mathrm{eco}} + \frac{3.5}{91.5} \cdot m_{\mathrm{eco}} + \frac{(0.357 \cdot \mathrm{CaO/SiO_2} - 0.404) \cdot 74.08\,\mathrm{g/mol} \cdot m_{\mathrm{eco}}}{56.08\,\mathrm{g/mol}}\right)}{\rho_{\mathrm{water}}} \end{aligned} \tag{2.31}$$

The calculation of the mass of the Ecocem will then be carried out as follows:

$$\begin{aligned} m_{\mathrm{eco}} = {} & \frac{V}{\frac{1}{\rho_{\mathrm{eco}}} + \frac{\frac{5.0}{91.5}}{\rho^{\mathrm{act}}_{\mathrm{Na_2CO_3}}} + \frac{\frac{3.5}{91.5}}{\rho^{\mathrm{act}}_{\mathrm{Ca(OH)_2}}} + \frac{(0.357 \cdot \mathrm{CaO/SiO_2} - 0.404) \cdot 74.08\,\mathrm{g/mol}}{56.08\,\mathrm{g/mol} \cdot \rho^{\mathrm{add}}_{\mathrm{Ca(OH)_2}}}} \\ & + \frac{V}{\frac{w/s \cdot \left(1 + \frac{5.0}{91.5} + \frac{3.5}{91.5} + \frac{(0.357 \cdot \mathrm{CaO/SiO_2} - 0.404) \cdot 74.08\,\mathrm{g/mol}}{56.08\,\mathrm{g/mol}}\right)}{\rho_{\mathrm{water}}}} \end{aligned} \tag{2.32}$$

2.1.4.4 Summary of all calculations

The results of all preparations used in this study are presented in the following two tables. Table 2.3 shows the percentage of weight of materials for each formulation. As can be seen in the Table 2.3, not only the water to solids ratio specified in ÖNORM EN 196-1[33] (water to solid ratio of 0.50) was used in this study. A second water to solid ratio of 0.66 was also utilized. As shown later in Section 3.2, the water to solid ratio was chosen as the lowest ratio where workability of all CaO/SiO_2 formulations was possible.

Tab. 2.3: Formulations of the materials used in this study in % of their mass * Ludox is composed by 50% water (H_2O) and 50% solid Ludox (SiO_2). dH_2O = distilled water.

			Alkali activated slag (AAS)					
	CaO/		**Slag**	**Activators**		**Additives**		**Water**
	SiO_2	w/s	Ecocem	Na_2CO_3	$Ca(OH)_2$	$Ca(OH)_2$	Ludox*	dH_2O
Norm	1.13	0.50	91.50%	5.00%	3.50%			50.00%
	0.50	0.66	64.77%	3.54%	2.48%		58.42%	36.79%
	0.80	0.66	80.59%	4.40%	3.08%		23.85%	54.07%
Reference	1.13	0.66	91.50%	5.00%	3.50%			66.00%
	1.50	0.66	78.95%	4.31%	3.02%	13.71%		66.00%

Tab. 2.4: Formulations of the materials used in this study in bases of 0.1 L * Ludox is composed by 50% water (H_2O) and 50% solid Ludox (SiO_2). dH_2O = distilled water.

			Alkali activated slag (AAS)					
	CaO/		**Slag**	**Activators**		**Additives**		**Water**
	SiO_2	w/s	Ecocem	Na_2CO_3	$Ca(OH)_2$	$Ca(OH)_2$	Ludox*	dH_2O
			g	g	g	g	g	g
Norm	1.13	0.50	108.13	5.91	4.14			59.09
	0.50	0.66	62.87	3.44	2.40		56.71	35.71
	0.80	0.66	79.32	4.33	3.03		23.48	53.22
Reference	1.13	0.66	90.94	4.97	3.48			65.59
	1.50	0.66	77.41	4.23	2.96	13.45		64.71

2.2 Methods

In the following subsections, all mixing procedures and quantities will be described. The tests will be discussed by starting from the fresh to the solid testing stages.

2.2.1 Cone-spread test

Two different cones were utilized in this study:

- mini Abrams cone [50] (shown in Figure 2.2a) used for spread tests, in Okamura (Section 2.2.2) and spread tests prior to vicat tests (Section 2.2.3). The value of τ_y was

also calculated from these cone spread tests (Section 1.4.1). The mini Abrams cone has a downsizing factor for each measurement of 5.26 to the standard Abrams cone of ÖNORM EN 12350-1 [32];

- european Guidelines cone for self-compacting concrete (SCC) [4] (shown in Figure 2.2b) used for the spread tests of the mortar pastes (i.e., higher paste volume).

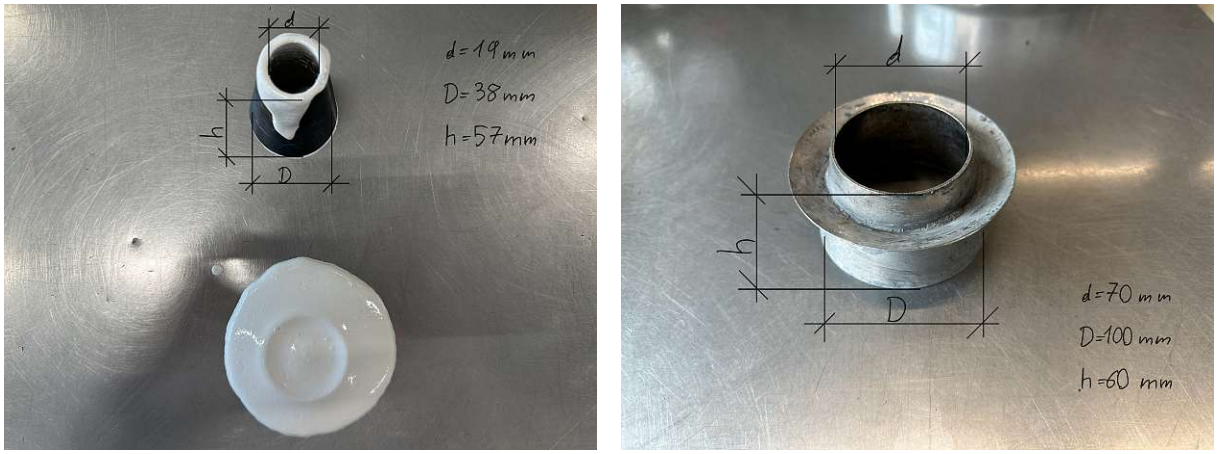

(a) Mini Abrams cone [50]. **(b)** European guideline cone [4].

Fig. 2.2: Cones spread tests.

The volume of each cone is calculated as follows:

$$\begin{aligned} V =& \frac{\pi \cdot h \cdot (r_{\text{top}}^2 + r_{\text{top}} \cdot r_{\text{bottom}} + r_{\text{bottom}}^2)}{3} \\ =& \frac{\pi \cdot h \cdot \left(\left(\frac{d_{\text{top}}}{2}\right)^2 + \left(\frac{d_{\text{top}}}{2}\right) \cdot \left(\frac{d_{\text{bottom}}}{2}\right) + \left(\frac{d_{\text{bottom}}}{2}\right)^2 \right)}{3} \end{aligned} \tag{2.33}$$

Three different batches of Ecocem were used in this study. In order to determine whether the batches have the same fresh properties, a spread test was performed over time for each batch. A spread test was also carried out on the batch used by Pudelko M. [39]. The exact test times and results are shown in the Appendix. The IKA overhead mixer shown in Figure 2.3 was used to mix the formulations. The testing procedure of the spread test was always the same. In the first step all solid parts:

- Ecocem (slag)
- Na_2CO_3 (activator)
- $Ca(OH)_2$ (activator/ additive)

were mixed together for ten seconds at a velocity of 1000 rpm in the right amount (see Table 2.5). Likewise, the liquid components (dH_2O and Ludox) were also mixed together for ten seconds at a velocity of 1000 rpm. After that the solid parts and the liquid parts were always mixed together using the mixing procedure described in Table 2.6. The spread test was carried out on pastes after mixing and over time, in order to characterize their hydration process. A decrease in spread is expected over time as the paste hydrates. In order to prevent evaporation, the mixtures

Tab. 2.5: Formulations of the materials for spread test: 0.1 L * Ludox is composed by 50% water (H_2O) and 50% solid Ludox (SiO_2). dH_2O = distilled water.

			Alkali activated slag (AAS)					
			Slag	**Activators**		**Additives**		**Water**
	CaO/SiO_2	w/s	Ecocem	Na_2CO_3	$Ca(OH)_2$	$Ca(OH)_2$	Ludox*	dH_2O
			g	g	g	g	g	g
Norm	1.13	0.50	108.13	5.91	4.14			59.09
	0.50	0.66	62.87	3.44	2.40		56.71	35.71
	0.80	0.66	79.32	4.33	3.03		23.48	53.22
Reference	1.13	0.66	90.94	4.97	3.48			65.59
	1.50	0.66	77.41	4.23	2.96	13.45		64.71

Fig. 2.3: Mixer: IKA STARVISC 200-2.5.

were kept covered between each spread test. Before testing the spread over time each paste was mixed at 1000 rpm for 1 minute (see Appendix).

Before doing the spread test, the table surface and the inside of each cone (see Figure 2.2) were slightly moistened. Next, the mixture was filled into the cone. Afterwards, the cone was lifted up within a timespan of one to two seconds to obtain a cake shape. The diameter of the spread was finally measured in two directions, and the average was calculated (as shown in Equation 1.7). In order to calculate the dynamic yield stress τ_y as presented in Equation 1.8, all the unknowns must first be determined:

- the volume of the mini Abrams cone [50] is 37.71 cm^3. The volume of the cone form the European guideline [4] is 344.00 cm^3;
- $\rho_{\text{total}} = \frac{m_{\text{eco}}+m^{\text{act}}_{\text{Na2CO3}}+m^{\text{act}}_{\text{Ca(OH)2}}+m_{\text{add}}+m_{\text{water}}}{V_{\text{T}}}$

Tab. 2.6: Spread and vicat tests mixing procedure.

Time	Operation	rpm
5 seconds	The liquids were added to the solid components	1000
85 seconds	Mixing	1000
Pause	The past was scraped from the outer surface of the container.	
90 seconds	Mixing	1000

The precise values for each CaO/SiO_2 and for each water to solid ratio are presented in Table 2.7.

Tab. 2.7: Values for calculating τ_y.

	Ca/Si	w/s	ρ_{total} (kg/m^3)	V_{water} (L)	V_{solid} (L)	V_{water}/V_{solid} -
Norm	1.13	0.50	1772.65	0.041	0.059	1.44
	0.50	0.66	1611.25	0.036	0.064	1.78
	0.80	0.66	1633.83	0.035	0.065	1.85
Reference	1.13	0.66	1649.79	0.034	0.066	1.91
	1.50	0.66	1627.55	0.035	0.065	1.83

The results are shown in Section 3.1.

2.2.2 Okamura test

To perform the Okamura test, a spread test for four different water to solid ratios is required for each CaO/SiO_2, so all the formulations shown in Table 2.8 were tested. In order to determine the value of β_p, it was necessary to calculate the relative slump flow (see Equation 1.9) and the ratio of V_{water} and V_{solid}. For the calculation of the relative slump flow, the average of two measured diameters (see Equation 1.7) and the top and bottom diameters of the mini Abrams cone (see Figure 2.2a) were inserted into the equation. The V_{water} can be calculated as follows for the different formulations:

$$V_{water} = \frac{\frac{100.0}{91.5} \cdot w/s \cdot m_{eco}}{\rho_{water}} \tag{2.34}$$

$$V_{water} = \frac{w/s \cdot \left(m_{eco} + \frac{5.0}{91.5} \cdot m_{eco} + \frac{3.5}{91.5} \cdot m_{eco}\right)}{\rho_{water}} + \frac{w/s \cdot 0.5 \cdot \frac{(m_{eco} \cdot 0.404 - CaO/SiO_2 \cdot m_{eco} \cdot 0.357) \cdot 2}{CaO/SiO_2} \cdot m_{eco}}{\rho_{water}} - \frac{0.5 \cdot \frac{(m_{eco} \cdot 0.404 - CaO/SiO_2 \cdot m_{eco} \cdot 0.357) \cdot 2}{CaO/SiO_2} \cdot m_{eco}}{\rho_{water}} \tag{2.35}$$

$$V_{water} = \frac{w/s \cdot \left(m_{eco} + \frac{5.0}{91.5} \cdot m_{eco} + \frac{3.5}{91.5} \cdot m_{eco} + \frac{(0.357 \cdot CaO/SiO_2 - 0.404) \cdot 74.08\,g/mol \cdot m_{eco}}{56.08\,g/mol}\right)}{\rho_{water}} \tag{2.36}$$

Tab. 2.8: Formulations of the materials for spread test: 0.1 L * Ludox is composed by 50% water (H_2O) and 50% solid Ludox (SiO_2). dH_2O = distilled water.

			Alkali activated slag (AAS)					
			Slag	**Activators**		**Additives**		**Water**
	CaO/SiO_2	w/s	Ecocem	Na_2CO_3	$Ca(OH)_2$	$Ca(OH)_2$	Ludox*	dH_2O
			g	g	g	g	g	g
	0.50	0.60	66.76	3.65	2.55		60.21	31.73
	0.50	0.66	62.87	3.44	2.40		56.71	35.71
	0.50	0.70	60.52	3.31	2.31		54.59	38.11
	0.50	0.75	57.82	3.16	2.21		52.15	40.87
	0.80	0.56	87.98	4.81	3.37		26.04	48.11
	0.80	0.57	87.03	4.76	3.33		25.76	48.67
	0.80	0.60	84.29	4.61	3.22		24.95	50.28
	0.80	0.66	79.32	4.33	3.03		23.48	53.22
Norm	1.13	0.50	108.13	5.91	4.14			59.09
	1.13	0.58	98.79	5.40	3.78			62.62
Reference	1.13	0.66	90.94	4.97	3.48			65.59
	1.13	0.70	87.46	4.78	3.35			66.91
	1.50	0.58	84.00	4.59	3.21	14.59		61.71
	1.50	0.66	77.41	4.23	2.96	13.45		64.71
	1.50	0.70	74.49	4.07	2.85	12.94		66.04
	1.50	0.75	71.13	3.89	2.72	12.36		67.57

Subsequently, the value of the V_{solid} can be calculated as follows:

$$V_{total} - V_{water} = V_{solid} \tag{2.37}$$

The results are presented in Table 2.9. Subsequently, a linear trend line is plotted, with the four points of each relative flow area Γ_m (x-axis) corresponding to a volume ratio of water to solid value (y-axis). The minimum amount of water referred to β_p is obtained for $\Gamma_m = 0$. The results are shown in Section 3.2.

2.2.3 Vicat test

The vicat test was performed in order to identify the initial and final setting points of the AAS pastes. For each vicat test, the overhead IKA mixer, which is shown in Figure 2.3, was used. For each test 0.25 L of mixture was prepared. All formulations which are shown in Table 2.10 were tested.

The testing procedure of the vicat test was always the same. In the first step all solid parts:

- Ecocem (slag)
- Na_2CO_3 (activator)
- $Ca(OH)_2$ (activator/ additive)

were mixed together for ten seconds at a velocity of 1000 rpm in the right amount (see Table 2.10). Likewise, the liquid components (dH_2O and Ludox) were also mixed together for ten seconds at

Tab. 2.9: Values for Okamura tests to calculate Γ_m (see Equation 1.9).

	Ca/Si	w/s	ρ_{total} (kg/m^3)	V_{water} (L)	V_{solid} (L)	$V_{\text{water}}/V_{\text{solid}}$ -
	0.50	0.60	1649.05	0.038	0.062	1.62
	0.50	0.66	1611.25	0.036	0.064	1.78
	0.50	0.70	1588.41	0.035	0.065	1.89
	0.50	0.75	1562.14	0.067	0.033	2.03
	0.80	0.56	1703.03	0.039	0.061	1.57
	0.80	0.57	1695.44	0.038	0.062	1.60
	0.80	0.60	1673.61	0.037	0.063	1.69
	0.80	0.66	1633.83	0.035	0.065	1.85
Norm	1.13	0.50	1772.65	0.041	0.059	1.44
	1.13	0.58	1705.91	0.037	0.063	1.68
Reference	1.13	0.66	1649.79	0.034	0.066	1.91
	1.13	0.70	1624.94	0.033	0.067	2.02
	1.50	0.58	1680.96	0.038	0.062	1.61
	1.50	0.66	1627.55	0.035	0.065	1.83
	1.50	0.70	1603.87	0.034	0.066	1.94
	1.50	0.75	1576.67	0.032	0.068	2.08

Tab. 2.10: Formulations of the materials for vicat test: 0.25 L * Ludox is composed by 50% water (H_2O) and 50% solid Ludox (SiO_2). dH_2O = distilled water.

			Alkali activated slag (AAS)					
			Slag	**Activators**		**Additives**		**Water**
	CaO/SiO_2	w/s	Ecocem	Na_2CO_3	$Ca(OH)_2$	$Ca(OH)_2$	Ludox*	dH_2O
			g	g	g	g	g	g
Norm	1.13	0.50	270.33	14.77	10.34			147.72
	0.50	0.66	157.17	8.59	6.01		141.77	89.27
	0.80	0.66	198.29	10.84	7.58		58.69	133.05
Reference	1.13	0.66	227.34	12.42	8.70			163.99
	1.50	0.66	193.52	10.57	7.40	33.62		161.77

a velocity of 1000 rpm. Following this step, the solid and liquid parts were always mixed together using the mixing procedure shown in Table 2.6. After mixing, a spread test was performed as described in Subsection 2.2.1. Then, the vicat test was carried out with the VICAMATIC-2 tester (see Figure 2.4a), which fulfills the requirements of ÖNORM EN 196-3 [35]. During the experiment:

- the room temperature was around 23° Celsius, which corresponds to a deviation of 2° from the tolerance range of (20.0 ± 1.0)°C from the ÖNORM EN 196-3 [35];
- the vicat apparatus was set up as follows:
  1. the timing of needle penetration was set (delay at start and time between needle penetrations). The start delay was set to be a little before the penetration depth

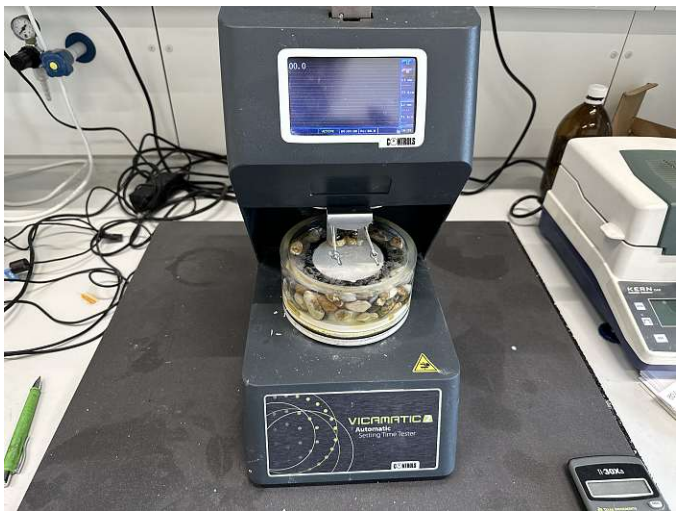

(a) VICAMATIC-2 tester from Controls.

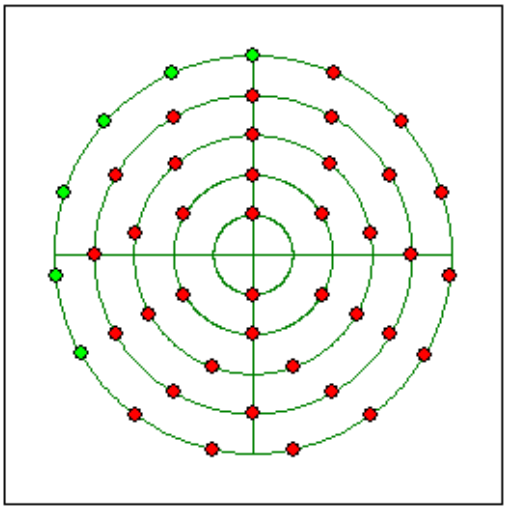

(b) Vicat test needle penetration points on the paste surface.

Fig. 2.4: VICAMATIC-2 tester from Controls and vicat test needle penetration points on the paste surface.

starts to decrease. The maximum number of points is 44. The maximum time between these points is about 109 minutes. After each needle drop, the VICAMATIC-2 tester automatically moves to the next point (see Figure 2.4b). It starts from the outermost circle and works its way forward with each revolution;

2. a transparent cylinder was placed on the VICAMATIC-2 tester. Within this cylinder, a black cone, referred to as the vicat ring, was put on. Then the vicat ring was filled with paste (see Figure 2.4a);
3. thereafter, the outer cylinder was filled with little stones and tap water. The stones were necessary to prevent the paste and the vicat ring from floating. The upper edge of the waterline was positioned at a minimum of 5 mm above the upper edge of the paste;
4. the needle was positioned in its designated starting position.

Then the actual test was initiated. The needle penetrated the paste in a predetermined time interval. The initial setting time was determined by measuring the time when the needle penetrated the paste to a depth of 37 to 31 mm. The final setting time, which represents the end of solidification, was reached when the needle penetrated the paste to a depth of 0.50 mm [35]. Two tests for each AAS pastes with different CaO/SiO_2 with the identical interval of the the needle drops were carried out. The average values and error bars of the penetration depth were calculated by using Equations 2.44 and 2.45.

2.2.4 Isothermal calorimetry test

Isothermal calorimetry tests were conducted to quantify the heat development of AAS pastes over time. The isothermal calorimeter (see Figure 2.5) always measures the heat development of the sample as a function of a reference as described in ÖNORM EN 196-11 [34]. The isothermal calorimeter tests required a lesser amount of material, thus a smaller mixer was utilized. The mixer used for this test was the IKA ULTRA TURRAX, shown in Figure 2.6a. The formulations tested

Fig. 2.5: Isothermal calorimeter TAM AIR TA instrument.

(a) IKA ULTRA TURRAX Tube Drive.

(b) IKA VORTEX 3.

Fig. 2.6: Mixer and vibration platform for preparing the mixtures for isothermal calorimetry.

are specified in Table 2.11. For isothermal calorimetry, the materials were prepared following the mixing procedure specified in Table 2.12. Immediately after mixing, 5.0 g of paste was poured into a first container and then vibrated for 30 seconds with the IKA VORTEX 3 (see Figure 2.6b) at level six. Immediately thereafter it was loaded into the calorimeter and the test was started. A second container with a total mass of 5.0 g was then filled, vibrated and loaded into the calorimeter in the same way. This mixing method follows the ÖNORM EN 196-11 [34] (method A - External mixing). The isothermal calorimeter was set at 20°C, as in ÖNORM EN 196-11 [34].

To calculate the mass of the reference (sand), the first step was to determine the total heat capacity (C_{total}) (see Equation 1.12). C_{total} is the sum of the mass of the components of the pastes multiplied by their specific heat capacity (c) (Table 2.11 and Table 2.13):

$$\begin{aligned} C_{\text{total}} = {} & 91.5\% \cdot (m_{\text{eco}} \cdot c_{\text{eco}}) + 5.0\% \cdot (m_{\text{Na}_2\text{CO}_3} \cdot c_{\text{Na}_2\text{CO}_3}) \\ & + 3.5\% \cdot (m_{\text{Ca(OH)}_2} \cdot c_{\text{Ca(OH)}_2}) \\ & + m_{\text{water}} \cdot c_{\text{water}} \\ & + m^{\text{add}}_{\text{SiO2}} \cdot c^{\text{add}}_{\text{SiO2}} \\ & + m^{\text{add}}_{\text{Ca(OH)}_2} \cdot c^{\text{add}}_{\text{Ca(OH)}_2} \end{aligned} \tag{2.38}$$

Tab. 2.11: Formulations for each container in the isothermal calorimetry test: 5.0 g * Ludox is composed by 50% water (H_2O) and 50% solid Ludox (SiO_2). dH_2O = distilled water.

			Alkali activated slag (AAS)					
			Slag	**Activators**		**Additives**		**Water**
	CaO/SiO_2	w/s	Ecocem	Na_2CO_3	$Ca(OH)_2$	$Ca(OH)_2$	Ludox*	dH_2O
			g	g	g	g	g	g
Norm	1.13	0.50	3.05	0.17	0.12			1.67
Reference	0.50	0.66	1.95	0.11	0.07		1.76	1.11
	0.80	0.66	2.43	0.13	0.09		0.72	1.63
	1.13	0.66	2.76	0.15	0.11			1.99
	1.50	0.66	2.38	0.13	0.09	0.41		1.99

Tab. 2.12: Isothermal calorimetry mixing procedure.

Time	Operation	RPM
10 seconds	The liquids were added to the solid components	400
170 seconds	Use a spatula to scrape the until it is well mixed	6000
90 seconds	Put 5 grams of total paste into the first container	
90 seconds	Put 5 grams of total paste into the second container	

Ecocem consists of several components (Table 2.1). To calculate Ecocem's specific heat capacity (c_{eco}), each component's percentage is multiplied by its specific heat capacity (c) (Table 2.13):

$$\begin{aligned} c_{eco} =& SiO_2 \cdot 35.7\% + CaO \cdot 40.4\% + Al_2O_3 \cdot 12.1\% + \\ & Fe_2O_3 \cdot 1.5\% + MgO \cdot 6.5\% + SO_3 \cdot 1.9\% + \\ & MnO \cdot 0.4\% + K_2O \cdot 0.5\% + Na_2O \cdot 0.3\% + TiO_2 \cdot 0.9\% \end{aligned} \tag{2.39}$$

$$\begin{aligned} c_{eco} =& 0.74 \cdot 35.7\% + 0.75 \cdot 40.4\% + 0.88 \cdot 12.1\% + \\ & 0.65 \cdot 1.5\% + 0.88 \cdot 6.5\% + 0.63 \cdot 1.9\% + \\ & 0.64 \cdot 0.4\% + 0.90 \cdot 0.5\% + 1.11 \cdot 0.3\% + 0.69 \cdot 0.9\% = 0.77 \end{aligned} \tag{2.40}$$

Now the masses from Table 2.11 and the heat capacities from Table 2.13 can be inserted into Equation 2.38 and the heat capacity of each sample can be calculated. For clarity reasons, the calculation without and with additives is listed below:

- without an additive

$$\begin{aligned} C_{total} =& 91.5\% \cdot (m_{eco} \cdot c_{eco}) \\ & + 5.0\% \cdot (m_{Na_2CO_3} \cdot c_{Na_2CO_3}) \\ & + 3.5\% \cdot (m_{Ca(OH)_2} \cdot c_{Ca(OH)_2}) \\ & + m_{water} \cdot c_{water} \end{aligned} \tag{2.41}$$

Tab. 2.13: Specific heat capacities and molar masses of AAS pastes chemical constituents.

Compound	Molar heat capacity $J \cdot mol^{-1} \cdot K^{-1}$	Molar mass $g \cdot mol^{-1}$	Specific heat capacity (c) $J \cdot g^{-1} \cdot K^{-1}$	Source
SiO_2	–	–	0.74	[19]
CaO	42.00	56.08	0.75	[42]
Al_2O_3	–	–	0.88	[25]
Fe_2O_3	103.90	159.69	0.65	[43]
MgO	–	–	0.88	[9]
SO_3	50.81	80.06	0.63	[26]
MnO	45.40	70.94	0.64	[45]
K_2O	84.53	94.20	0.90	[44]
Na_2O	69.10	61.98	1.11	[46]
TiO_2	55.00	79.87	0.69	[47]
Na_2CO_3	111.30	105.99	1.05	[16]
$Ca(OH)_2$	87.50	74.08	1.18	[41]
H_2O	–	–	4.18	
Sand	–	–	0.76	

- with Ludox (additive)

$$\begin{aligned} C_{\text{total}} = {} & 91.5\% \cdot (m_{\text{eco}} \cdot c_{\text{eco}}) \\ & + 5.0\% \cdot (m_{Na_2CO_3} \cdot c_{Na_2CO_3}) \\ & + 3.5\% \cdot (m_{Ca(OH)_2} \cdot c_{Ca(OH)_2}) \\ & + \left(m_{\text{water}} + \frac{m^{\text{add}}_{\text{Ludox, total}}}{2} \right) \cdot c_{\text{water}} \\ & + \frac{m^{\text{add}}_{\text{Ludox, total}}}{2} \cdot c^{\text{add}}_{\text{SiO2}} \end{aligned} \tag{2.42}$$

- with $Ca(OH)_2$ (additive)

$$\begin{aligned} C_{\text{total}} = {} & 91.5\% \cdot (m_{\text{eco}} \cdot c_{\text{eco}}) \\ & + 5.0\% \cdot (m_{Na_2CO_3} \cdot c_{Na_2CO_3}) \\ & + 3.5\% \cdot (m_{Ca(OH)_2} \cdot c_{Ca(OH)_2}) \\ & + m_{\text{water}} \cdot c_{\text{water}} \\ & + m^{\text{add}}_{\text{Ca(OH)2}} \cdot c^{\text{add}}_{\text{Ca(OH)2}} \end{aligned} \tag{2.43}$$

The amount of reference sand corresponding to the same heat capacity of the AAS formulations is listed in Table 2.14.

2.2.5 Mortar prisms

The mortar prisms were made to test the flexural and compressive strength of several AAS formulations over time. For the production of the mortar prisms, the Hobart mortar mixer, as described in ÖNORM EN 196-1 [33] and shown in Figure 2.7a, was used. Unlike previous tests,

Tab. 2.14: Heat capacities for all AAS formulations and their references (sand).

	CaO/SiO_2	w/s	Heat capacity C_{total} $J \cdot K^{-1}$	Mass of sand (reference) g
Norm	1.13	0.50	9.63	12.67
	0.50	0.66	10.67	14.04
	0.80	0.66	10.69	14.07
Reference	1.13	0.66	10.71	14.10
	1.50	0.66	10.75	14.31

mortar prisms consist not only of slag, activators, additives, and water, but also of sand. The weight ratio of sand to the solid components of the mixture is 1:3. Therefore, sand was sieved

(a) Horbat mortar mixer.

(b) Vibration platform beckel B 3000.

Fig. 2.7: Mixer and vibration platform for preparing AAS prisms.

according to ÖNORM EN 196-1 [33]. Once all the components were prepared, the first step was

Tab. 2.15: Formulations of the materials for 30 prisms: 0.96 L * Ludox is composed by 50% water (H_2O) and 50% solid Ludox (SiO_2). dH_2O = distilled water.

			Alkali activated slag (AAS)						
			Slag	**Activators**		**Additives**		**Water**	**Sand**
	CaO/SiO_2	w/s	Ecocem g	Na_2CO_3 g	$Ca(OH)_2$ g	$Ca(OH)_2$ g	Ludox* g	dH_2O g	g
Norm	1.13	0.50	444.03	24.26	16.98			242.64	1455.82
	0.50	0.66	287.56	15.71	11.00		259.38	163.33	1331.90
	0.80	0.66	360.15	19.68	13.78		106.60	241.66	1340.73
Reference	1.13	0.66	410.80	22.45	15.71			296.32	1346.89
	1.50	0.66	352.20	19.25	13.47	61.18		294.42	1338.29

to combine all the solid parts, as shown in Table 2.15 in the bucket:

- Ecocem (slag)
- Na_2CO_3 (activator)

- $Ca(OH)_2$ (activator/ additive)

They were then mixed together at low speed for ten seconds. Likewise, the liquid components (dH_2O and Ludox) were also mixed together for ten seconds at a low speed. The mixing procedure is described in Table 2.16. During the pause, after the first minute of mixing, and before adding the sand, a spread test was also done. The results of these spread tests are presented in Section 3.1. After mixing, the paste was put into demoldable plexiglass molds. As shown in Figure 2.8, each

Tab. 2.16: Mixing procedure for mortar prisms.

Time	Operation
10 seconds	Addition of the liquids to the solid components
30 seconds	Slow mixing of the paste
30 seconds	Fast mixing of the paste
Pause	Scraping down the paste + spread test
60 seconds	Slow mixing while sand is added
60 seconds	Fast mixing of the mortar

prism has dimensions of 2 x 2 x 8 = 32 cm^3. It was decided to use reduced prisms (volume = 32 cm^3) instead of standard prisms according to ÖNORM EN 196-1 EN [33] (4 x 4 x 16 = 256 cm^3). Pudelko M. [39] demonstrated that the same results could be achieved with the same material when using the scaled down versions. Afterwards, each mold was placed onto the vibration platform, beckel B 3000 (see Figure 2.7b) for 30 seconds. Then the top edge was leveled with a spatula. The storage conditions will be discussed in following Subsection 2.2.5.1.

Fig. 2.8: Prisms in the 2 x 2 x 8 cm^3 plexiglass molds covered with plastic foil.

2.2.5.1 Mortar prisms storage conditions

The freshly poured mortar prisms, together with the formwork, were stored for one day at room temperature under a plastic wrapping foil. As described in ÖNORM EN 196-1 EN [33], the prisms were demolded after one day and partially stored above and below water, as illustrated in Figure 2.9. In order to prevent leakage, the latter was saturated with Ecocem (6.0 g/L). The prisms with a CaO/SiO_2 of 0.50 exhibited partial dissolution in the water within one hour. Consequently, the prisms with CaO/SiO_2 of 0.50 and 0.80 were placed above the water for the first six days. Subsequently, the prisms were submerged in water. The containers were stored in a climate chamber in order to secure a constant temperature and humidity level. The storage conditions in the climate chamber were set at 23 °C and 65 % Relative Humidity (RH).

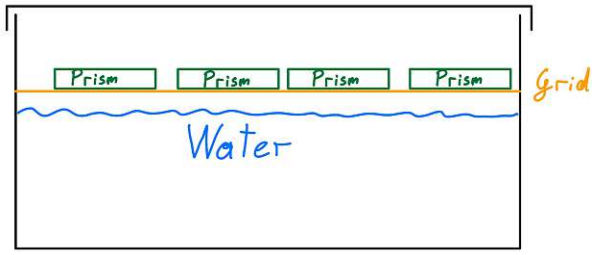

(a) Sketch storage above water.

(b) Actual storage above water.

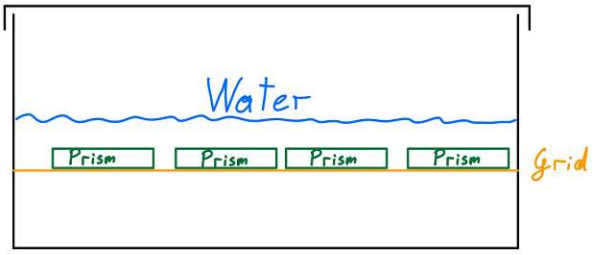

(c) Sketch storage under water.

(d) Actual storage under water.

Fig. 2.9: Mortar prisms storage conditions in the climate chamber.

2.2.5.2 Mortar prisms testing

In accordance with ÖNORM EN 196-1 EN [33], three prisms were prepared for each day of testing. The tests were conducted after 1, 7, 14, 28, 56 and 112 days above water (6 x 3 = 18 prisms) and after 7, 28, 56 and 112 days below water (4 x 3 = 12 prisms). Therefore, a total of 30 prisms were produced for each AAS formulation (see Table 2.15). The test procedures were performed according to the following protocol:

1. each prism was tested before with the three-point bending configuration to determine flexural strength (see Figure 2.10a). At the point of failure, each prism broke into two halves;

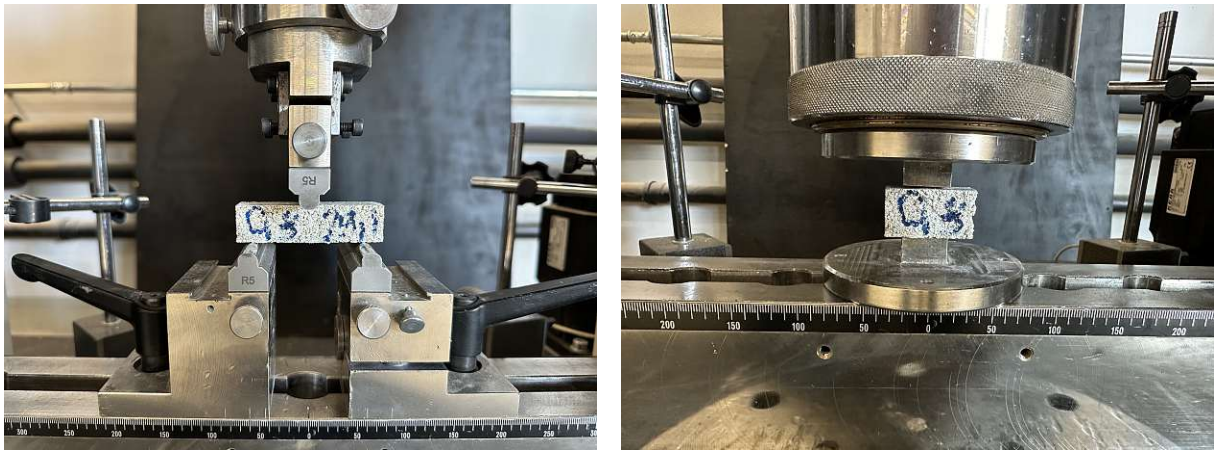

(a) 3-point bending strength test configuration. **(b)** Compressive strength test configuration.

Fig. 2.10: Mortar prism mechanical testing made with Zwick Roell Z250 machine.

2. each of the two resulting halves was then subjected to a compressive strength test (see Figure 2.10b).

The two experiments are also discussed in detail below. To perform both tests, the Zwick Roell Z250 machine was used in combination with the testXpert III-1.6 software.

Flexural strength mechanical testing

A three-point bending test was carried out using a Zwick Roell Z250 machine (see Figure 2.10a) on 2 x 2 x 8 cm^3 prisms. The test procedure is the following:

- each mortar prism was positioned so that its longitudinal axis was perpendicular to the rollers as described in ÖNORM EN 196-1 EN [33],
- the distance between the support rollers (the bottom two) was 6.0 cm, which deviates from the ÖNORM EN 196-1 EN [33], where the distance is described as 10 cm for 4 x 4 x 16 cm^3,
- the upper load roller, which applies the load, was positioned in the middle parallel to the support rollers as described in ÖNORM EN 196-1 EN [33].

Previous tests conducted by Aschauer C. [2] and Pudelko M. [39] used the same material and the same scaled down prism size. Throughout the preliminary testing, the pre-load and load increase were determined through an iterative process. Specifically, the preload was set at 20 N, and the load increase was set at 6 N/s. In order to ensure the comparability of the previous results, these two parameters were maintained constant throughout the subsequent tests, unless a failure occurred before the preload was reached, in which case the testXpert III-1.6 software did not determine a flexural strength value. As a result, the preload was not applied to the remaining prisms in the test series. This applies to the following tests:

- $CaO/SiO_2 = 0.50$:
  - above water: 1 day

  - under water: 7, 28 days

- $CaO/SiO_2 = 0.80$:
  - above water: 1 day
  - under water: 7 days

Flexural strength is calculated using the Equation 1.13

Compressive strength mechanical testing
As previously discussed in Subsection 2.2.5.2, each prism was split into two halves after the flexural test. Afterwards, the three rollers for the flexural test were removed from the Zwick Roell Z250 and the setting for the compressive test was inserted. In accordance with ÖNORM EN 196-1 [33], the dimensions of the pressure plates on the top and bottom of the prisms were 4.0 x 4.0 cm, resulting in a area of 16.0 cm^2. As the study employed scaled-down prisms, the pressure plates were also scaled down to a size of 2.0 x 2.0 cm = 4.0 cm^2. The prisms were positioned in the center between the two pressure plates. Each prism was oriented so that the more irregular top of the prisms (see Figure 2.8) faced the tester (see Figure 2.10b). The preload was set at 50 N, while the load increase was set at 0.30 MPa/s = $N/mm^2/s$. However, if a failure occurred before reaching the preload, the testXpert III-1.6 software would not determine a compressive strength value. As a result, the preload was not applied to the remaining prisms in the test series. This applies to the following tests:

- $CaO/SiO_2 = 0.50$:
  - above water: 1 day
- $CaO/SiO_2 = 0.80$:
  - above water: 1 day

The compressive strength is calculated using Equation 1.14

2.2.6 Overview of all tests

All tests performed in this study are summarized in Table 2.17. For all tests, the averages are calculated as follows:

$$\bar{x} = \frac{1}{n}\sum_{i=1}^{n} x_i \tag{2.44}$$

The standard deviation for all tests is calculated as follows:

$$\sigma = \sqrt{\frac{1}{n}\sum_{i=1}^{n}(x_i - \bar{x})^2} \tag{2.45}$$

Tab. 2.17: Summary of tests performed in this thesis. Spread tests were performed to calculate the minimum water demand (i.e., Okamura) and the dynamic yield stress τ_y of the main formulation (i.e., w/s = 0.66 and w/s= 0.50). * The prisms were stored above water until the sixth day, then placed under water.

			Spread	**Vicat**	**Calorimetry**	**Prisms above water**						**Prisms under water**			
						1d	7d	14d	28d	56d	112d	7d	28d	56d	112d
	CaO/SiO_2	**w/s**													
Norm	1.13	0.50	x	x	x	x	x	x	x	x	x	x	x	x	x x
	0.50	0.66	x	x	x	x	x	x	x	x	x		x*	x*	x*
	0.80	0.66	x	x	x	x	x	x	x	x	x		x*	x*	x*
Reference	1.13	0.66	x	x	x	x	x	x	x	x	x		x	x	x
	1.50	0.66	x	x	x	x	x	x	x	x	x		x	x	x
	0.50	0.60	x												
	0.50	0.70	x												
	0.50	0.75	x												
	0.80	0.56	x												
	0.80	0.57	x												
	0.80	0.60	x												
	1.13	0.58	x												
	1.13	0.70	x												
	1.50	0.58	x												
	1.50	0.70	x												
	1.50	0.75	x												

Chapter 3

Results and discussion

The following chapter shows and discuss the results of the tests which have been described in the previous chapter.

3.1 Spread tests

The spread tests were performed with the mini Abrams cone [50] and the cone from the European guideline [4] (see Figure 2.2) to compare the spread and dynamic yield stress of AAS pastes with different CaO/SiO_2 at the same w/s ratio of 0.66. Additional tests were also performed for the reference AAS paste with a $CaO/SiO_2 = 1.13$ at w/s of 0.50. Spread tests were also performed for each CaO/SiO_2 at various w/s (see Table 2.17) for the Okamura tests. These results are presented in the following Subsection 3.2. The main focus in this section is to compare the spread of all the CaO/SiO_2 at a w/s of 0.66 and the $CaO/SiO_2 = 1.13$ at a w/s of 0.50 (Norm). The

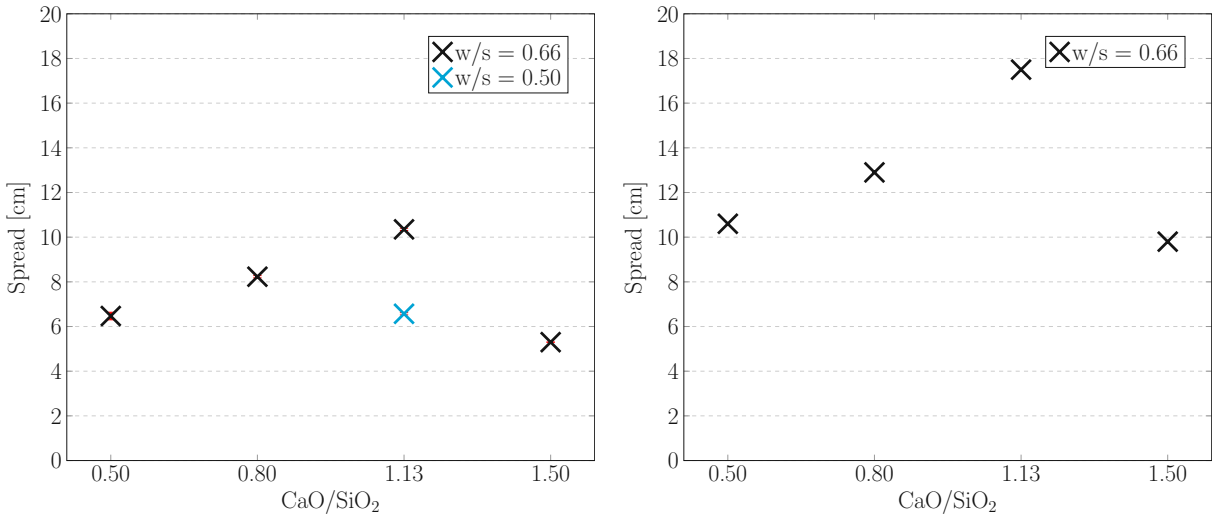

(a) Initial spread at different w/s ratios with the mini Abrams cone [50] (see Figure 2.2a). Each marker shows the average from three different spread tests.

(b) Initial spread with the cone from the European Guidelines [4] (see Figure 2.2b). Each marker shows the result from one spread test.

Fig. 3.1: Initial spread at different w/s ratios with mini Abrams cone [50] (**a**) and with the cone from the European guideline [4] (**b**). Ecocem has $CaO/SiO_2 = 1.13$. The other different CaO/SiO_2 are obtained by adding: Ludox for 0.50 and 0.80 and $Ca(OH)_2$ for 1.50.

exact test procedure is described in Subsection 2.2.1.

Both graphs in Figure 3.1 show the spread immediately after mixing. Figure 3.1a shows the results of the spread test with the mini Abrams cone [50] and Figure 3.1b shows the results from the cone from the European Guidelines [4]. The x-axis shows the different CaO/SiO_2. The y-axis shows the spread of the mixes in centimeters. In Figure 3.1b there is no average and no standard deviation as only one test was performed for each of the different CaO/SiO_2 of the AAS formulations. Comparing both results for the w/s = 0.66 shown in Figure 3.1, it can be seen that the trend of the spread with the different CaO/SiO_2 is the same for both cones. Figure 3.2 shows the dynamic yield stress τ_y (see Section 1.4.1) calculated from the spread immediately after mixing. The x-axis shows the different CaO/SiO_2. The y-axis shows the τ_y of the mixtures in Pa. The standard deviation of the spread is very small (see Figure 3.1a) and consequently the

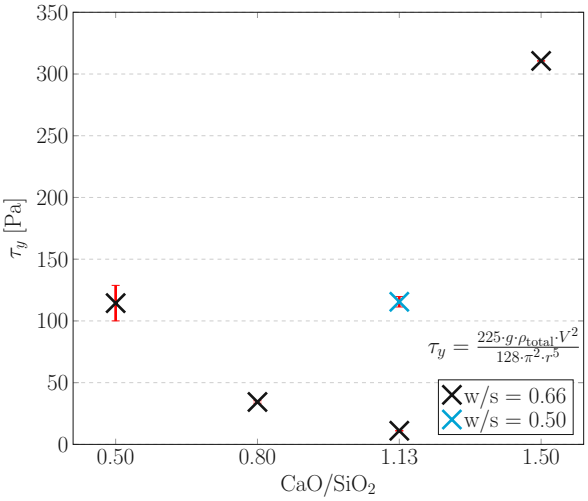

(a) τ_y at different w/s ratios from the mini Abrams cone [50] (see Figure 2.2a). Each marker shows the average calculated from three different spread tests.

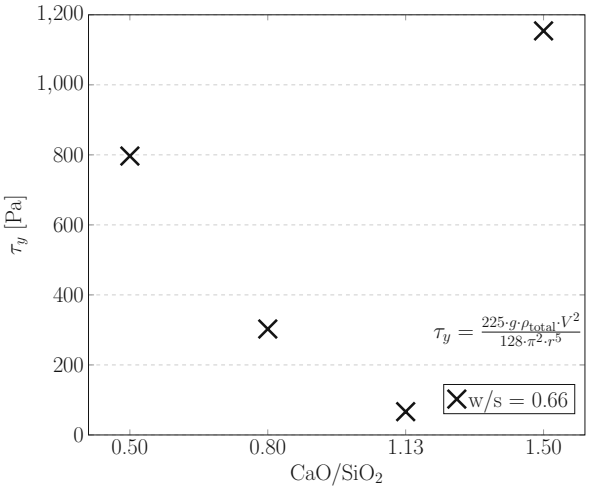

(b) τ_y from the cone from the European Guidelines for [4] (see Figure 2.2b). Each marker shows the calculation from one spread test.

Fig. 3.2: Dynamic yield stress, τ_y, at different w/s ratios calculated from mini Abrams cone [50] (**a**) and from the cone from European guideline [4] (**b**). Ecocem has CaO/SiO_2 = 1.13. The other different CaO/SiO_2 are obtained by adding: Ludox for 0.50 and 0.80 and $Ca(OH)_2$ for 1.50.

error bar of the τ_y is also small. In Figure 3.2b there is no average and no standard deviation because the spread tests are only done once for each CaO/SiO_2 (see Figure 3.1b).

The spread and the dynamic yield stress do not have a specific trend in correspondence with the CaO/SiO_2. The largest spread and thus the lowest τ_y is achieved by the reference AAS paste with a CaO/SiO_2 of 1.13. Followed by the CaO/SiO_2 of 0.80, 0.50. The lowest spread (the highest τ_y) is reached by the AAS paste with a CaO/SiO_2 of 1.50. All the last three ratios have in common that some additives are added. Ludox®TM-50 colloidal silica, which is a nano dispersed solution in water for CaO/SiO_2 of 0.50 and 0.80. Calcium hydroxide, which is a fine powder for the CaO/SiO_2 of 1.50. The nano dispersed and fine powders have in common that they have a large specific surface area in comparison with Ecocem grains. Therefore, these pastes are very water demanding and cohesive. As a result, the workability of the different CaO/SiO_2 varies. Comparing the two results for the w/s = 0.66 shown in Figure 3.2, it can be seen that the calculated τ_y from the two different cones does not match. This can be due to different mixing procedures, intensities, volumes, and duration when the spread test is performed (see Table 2.6

and Table 2.16). Tan et al. [50] show that different spreads are obtained by different mixing procedures.

3.2 Okamura tests

The Okamura test is performed to find the minimum water demand of a paste (i.e., β_p) [29]. To obtain the β_p for each CaO/SiO_2, four spread tests at different w/s must be performed. Then the relative slump flow Γ_m for each CaO/SiO_2 of each of the four spreads (see Figure 3.3) can be calculated using Equation 1.9. Each w/s also has a ratio of the volume of water to

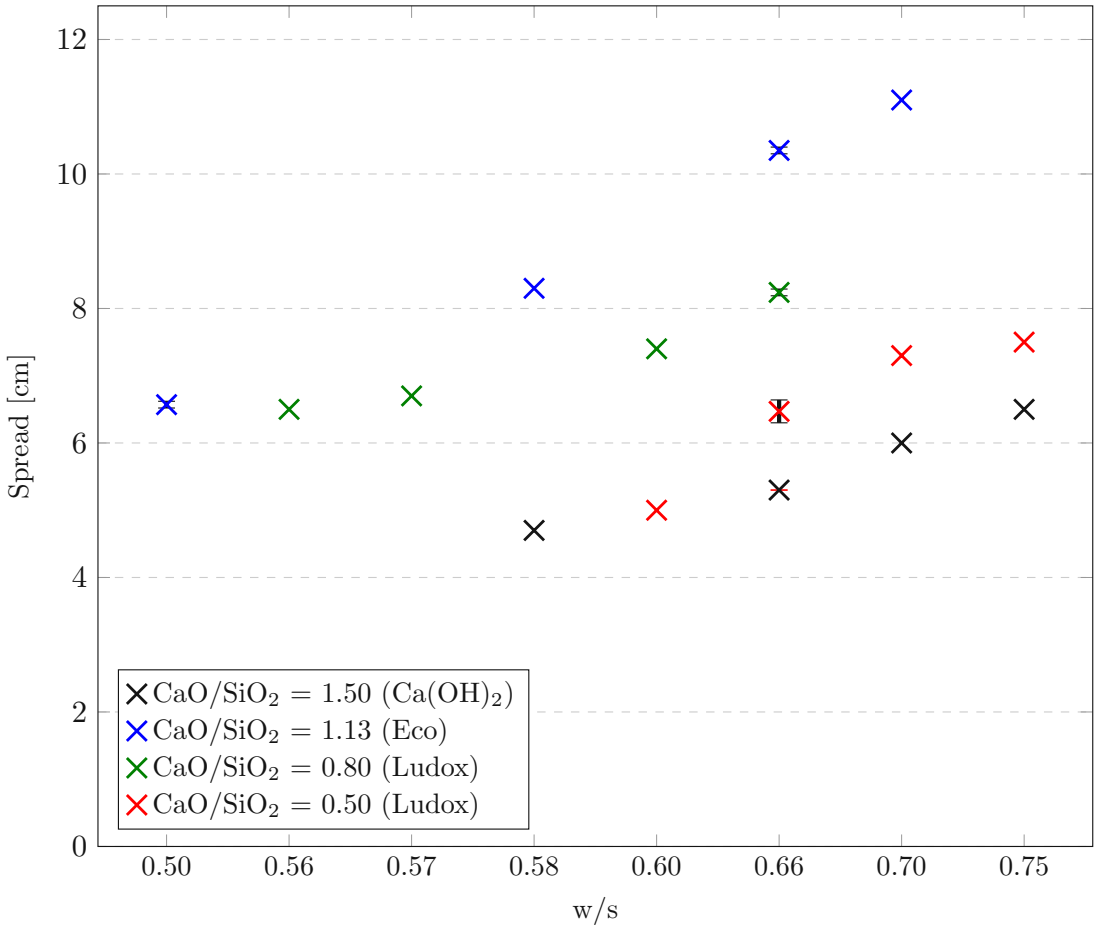

Fig. 3.3: Initial spread at various CaO/SiO_2 and various w/s ratios for the Okamura test. Each marker at a w/s of 0.50 and 0.66 shows the average of three different spread tests. All other markers are from one spread test each.

the volume of solid. This is calculated as shown in Subsection 2.2.2. The results are given in Table 2.7. Figure 3.4 shows the relationship between the relative slump flow Γ_m on the x-axis and the V_{water}/V_{solid} for each CaO/SiO_2 at each w/s. Figure 3.4 also shows four linear trend lines through the four markers for each CaO/SiO_2, as well as their equations. From the linear trend lines we can estimate β_p ($\Gamma_m = 0$) and the sensitivity of the formulations. It can be seen that the β_p is not a function of the CaO/SiO_2. The lowest β_p is reached for the AAS paste with a $CaO/SiO_2 = 1.13$ followed by $CaO/SiO_2 = 0.80$. The highest β_p is reached by two AAS pastes at CaO/SiO_2 0.50 and 1.50. As already mentioned the additive calcium hydroxide as well as the

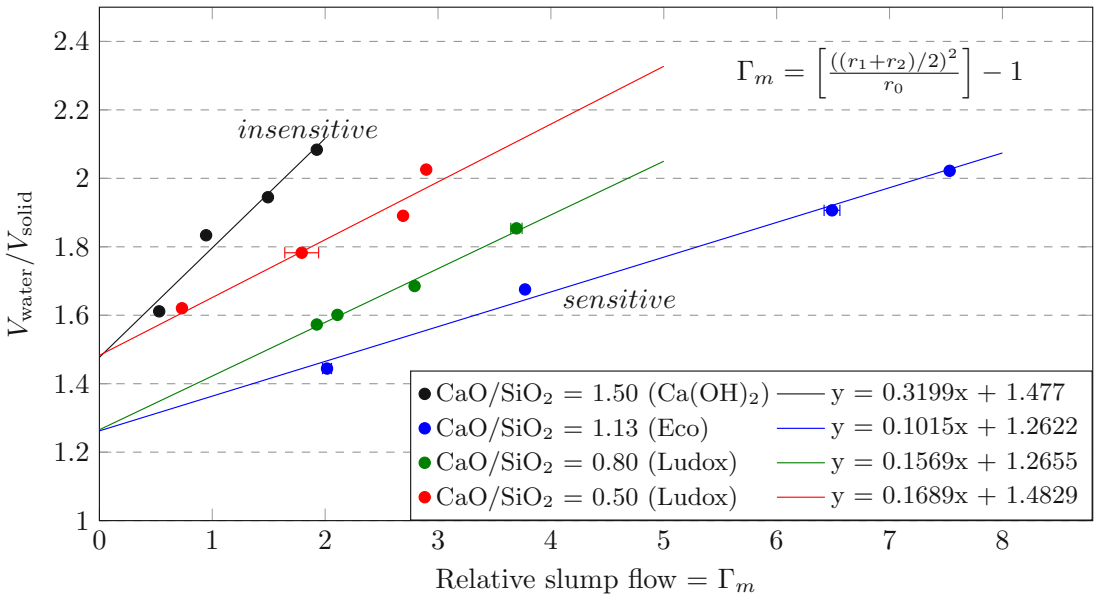

Fig. 3.4: Okamura results for AAS pastes with different CaO/SiO_2. The relative slump flow Γ_m is calculated using Equation 1.9. The slope of the line interpolation between the points represents the sensitivity of each AAS paste. From the linear trend lines we can estimate β_p ($\Gamma_m = 0$).

nano dispersed solution of Ludox have very fine particle size and a large specific surface area. This indicates that a greater amount of finer particles and a specific surface area increase the water demand of the pastes. The slope of the equations shows how sensitive the mixtures are, according to the Okamura [27] method. A steeper line indicates an insensitive mixture, while a flatter line indicates a sensitive mixture. Again, the slope is not a function of CaO/SiO_2, but follows the order of β_p. The AAS paste with a $CaO/SiO_2 = 1.13$ has the lowest slope and is the most sensitive formulation. The least sensitive mixture is the AAS paste with a $CaO/SiO_2 = 1.50$ where $Ca(OH)_2$ is used as an additive.

This observation indicates that the addition of all additives, especially calcium hydroxide, leads to a reduction in the sensitivity of the mixture as well as an increase in the water demand. This could be of interest for future optimization of self-compacting properties.

3.3 Vicat tests

The vicat test is performed to determine the initial and final setting time of each AAS paste at different CaO/SiO_2. Two separate tests are performed for each CaO/SiO_2. As described in Subsection 2.2.3, for each test, the paste is poured into a 40.0 mm high cone placed in a cylinder. This cylinder is filled with water up to at least 5 mm above the top of the paste. The cylinder is placed on the VICAMATIC-2 tester, which automatically measures the penetration depth of the needle into the paste at preset intervals. The time at which a penetration of 37.0 - 31.0 mm occurs is the time at which the initial setting point (t_{start}) occurs. The final setting time (t_{end}) occurs at a penetration of 0.50 mm as described in ÖNORM EN 196-3 [35].

Figure 3.5 shows the results of the vicat tests. The yellow areas are the zones of the initial (37.0 - 31.0 mm) and final (0.5 - 0.0 mm) setting points. The x-axis represents the age of each paste in hours, while the y-axis shows the penetration depth in mm. It can be seen that the AAS pastes with $CaO/SiO_2 = 1.13$ at a w/s = 0.50 and 0.66 as well as the $CaO/SiO_2 = 1.50$ at a

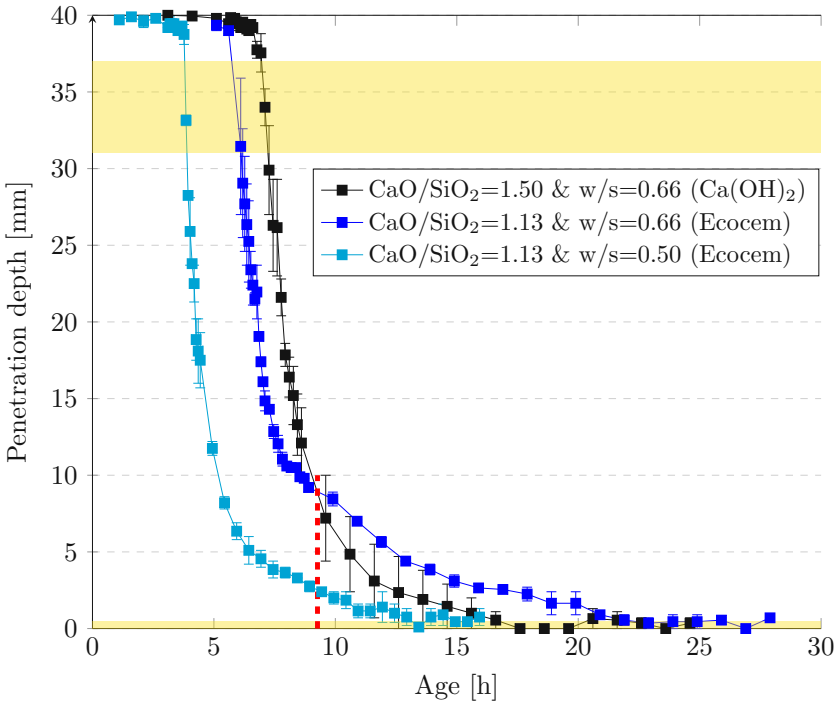

(a) AAS pastes with a $CaO/SiO_2 = 1.50$ at w/s = 0.66 and $CaO/SiO_2 = 1.13$ at w/s = 0.50 and w/s = 0.66.

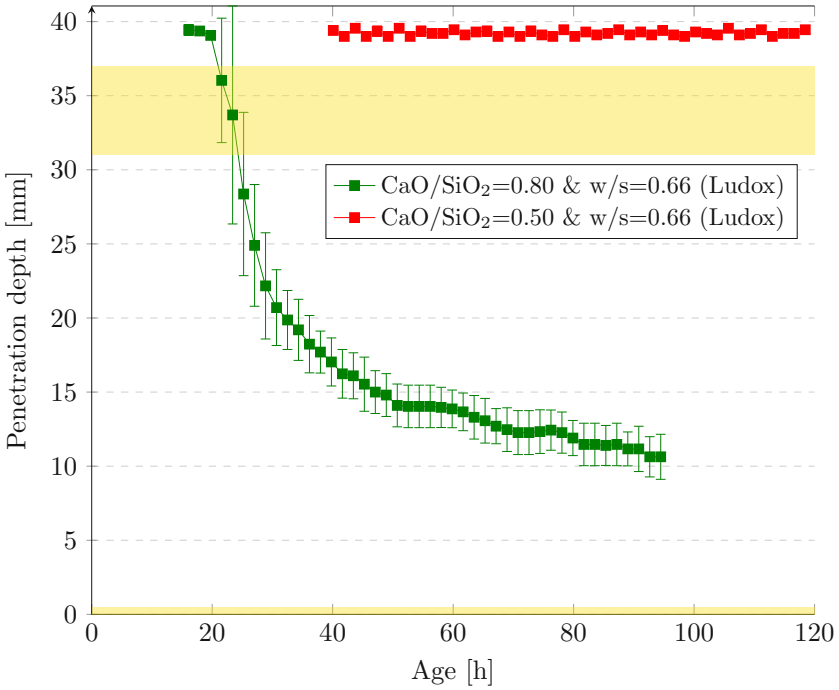

(b) AAS pastes with a $CaO/SiO_2 = 0.80$ at w/s = 0.66 and $CaO/SiO_2 = 0.50$ at w/s = 0.66.

Fig. 3.5: Results of the vicat tests. Each marker represents the average of two tests ($\bar{x} = \frac{x_{max}+x_{min}}{2}$). The yellow areas represent the initial (37-31 mm) and final (0.5-0 mm) setting phases.

w/s = 0.66 shown in Figure 3.5a have a final setting time within the first 24 hours. Figure 3.5b shows both AAS pastes with CaO/SiO_2 of 0.50 and 0.80 where Ludox is used as an additive. The initial setting time of CaO/SiO_2 = 0.80 occurs around 22:39 ± 01:40 hours. The initial setting of CaO/SiO_2 = 0.50 instead does not occur in the entire test. Table 3.1 summarizes the initial and final setting times for all AAS pastes at different CaO/SiO_2.

Tab. 3.1: Initial and final setting time for all AAS pastes from vicat tests (two for each formulations).

Ca/SiO_2	w/s	Initial setting time t_{start} [h]	Final setting time t_{end} [h]
■ 1.13	0.50	03:51 ± 00:03	14:53± 00:49
■ 1.50	0.66	07:06 ± 00:08	16:42 ± 01:00
■ 1.13	0.66	05:56 ± 00:12	22:09 ± 02:28
■ 0.80	0.66	22:39 ± 01:40	Not reached in the tests (120 h)
■ 0.50	0.66	Not reached in the tests (120 h)	Not reached in the tests (120 h)

A comparison of AAS pastes with CaO/SiO_2 = 1.13 with a w/s = 0.50 and w/s = 0.66 shows that a higher amount of water in the paste delays the initial and final setting times (see Figure 3.5a), as expected. A comparison of AAS pastes with CaO/SiO_2 1.13 and 1.50 at a w/s = 0.66 (Figure 3.5a) reveals that the AAS paste with CaO/SiO_2 of 1.50 has a later initial setting point but an earlier final setting point. This indicates that the addition of calcium hydroxide accelerates the hydration process after approximately 9:15 hours of contact with water. The initial setting point for AAS pastes with CaO/SiO_2 0.80 and w/s = 0.66 is reached more or less after one day (see Table 3.1). The initial setting point at CaO/SiO_2 = 0.50 and w/s = 0.66 is not reached during the explored time range in the test. Both end points for AAS pastes with CaO/SiO_2 = 0.50 and 0.80 are not reached during the time range explored in the test. The addition of Ludox (i.e., SiO_2) delays the setting in comparison to systems richer in calcium (i.e. CaO/SiO_2 1.13 and 1.50). In OPC pastes the setting starts at the earliest after one hour and finishes at the latest after 12 hours [5]. The setting times of AAS formulations with CaO/SiO_2 ratios of 1.13 and 1.50 are more comparable to those of OPC, even if they are delayed.

3.4 Isothermal calorimetry tests

Isothermal calorimetry is performed to measure the heat of hydration of pastes developed over time (see Figure 2.5) as a function of an inert reference. For this purpose, the total heat capacity (C_{total}) of the pastes is calculated together with the required mass of reference (sand) (see Subsection 2.2.4). Two tests are performed for each AAS paste at different CaO/SiO_2.

The results of the isothermal calorimetry tests are shown in Figure 3.6 and 3.8, for the heat evolution over time, and Figure 3.7, for the accumulated heat over the entire test duration. Figure 3.6a shows the normalized heat flow per gram of total AAS paste weight (Table 2.11) for AAS pastes with CaO/SiO_2 = 1.13 at w/s = 0.50 and 0.66. Figure 3.6b shows the normalized heat flow per gram of total AAS paste weight (Table 2.11) for all AAS formulations at w/s = 0.66. In Figure 3.6, the x-axis shows the age of the mixtures in days, and the y-axis shows the watts per gram of the total weight of the pastes. The same curves are also shown separately for each CaO/SiO_2 in Figure 3.8, with a zoom on the first 48 hours of AAS paste aging. The vertical colored areas represent the time between the initial and final settings of the vicat tests (see Table 3.1). The increase in the heat of hydration indicates an ongoing exothermic reaction. The peak of the heat of hydration for AAS with a CaO/SiO_2 = 1.13 at a w/s = 0.50 occurs at

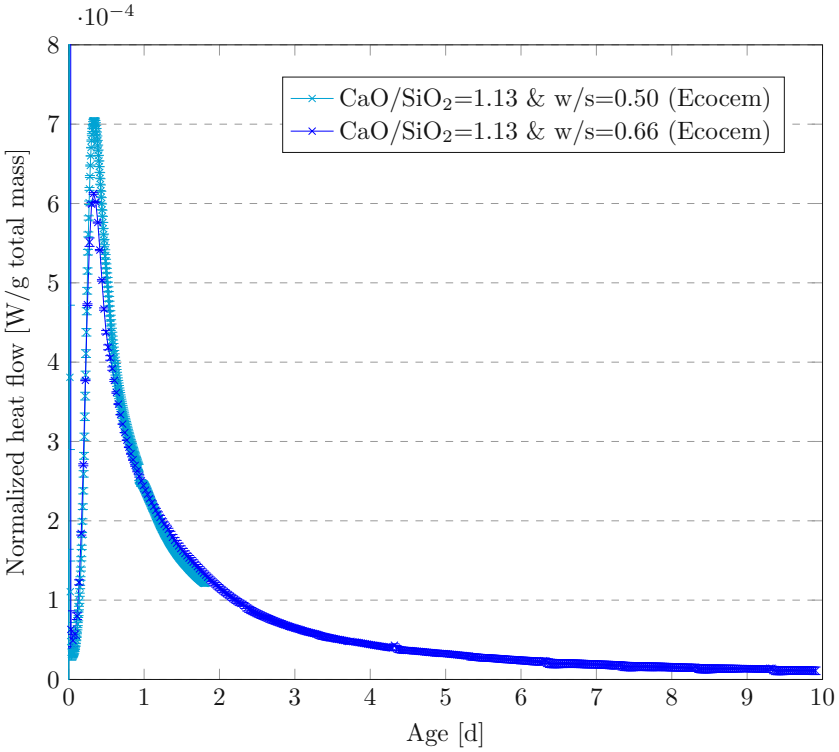

(a) AAS paste with a $CaO/SiO_2 = 1.13$ at a $w/s = 0.50$ (light blue) and 0.66 (blue).

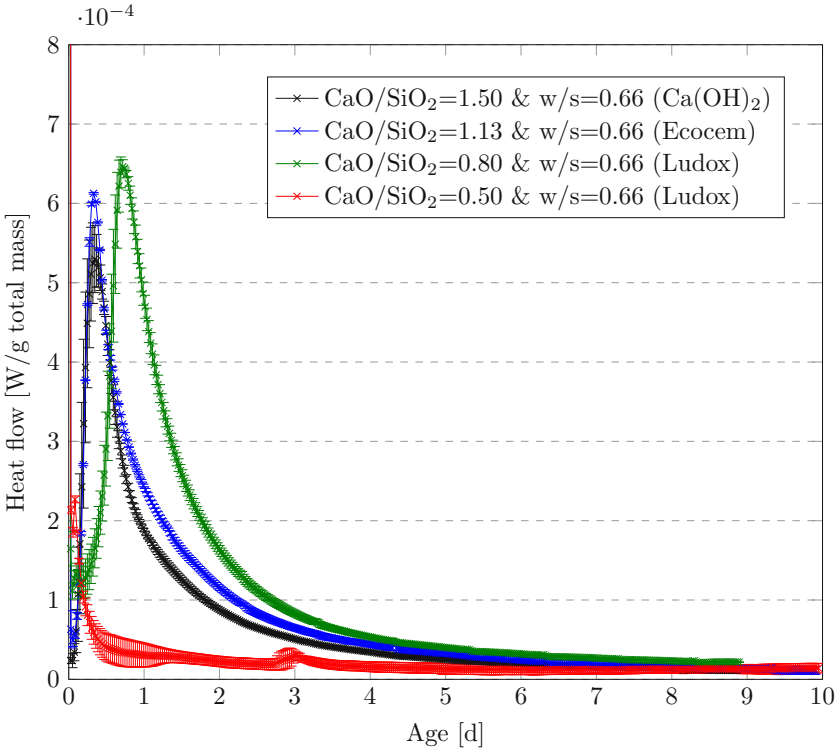

(b) AAS paste with different CaO/SiO_2 at a $w/s = 0.66$.

Fig. 3.6: Normalized heat flow (per gram of total AAS paste weight) as a function of time for AAS pastes with different CaO/SiO_2.

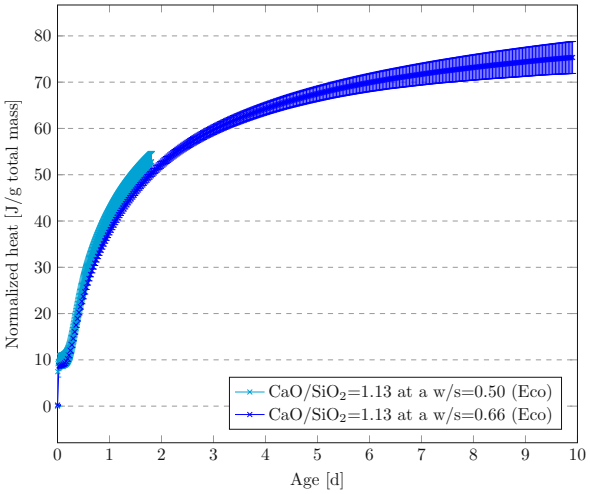

(a) AAS paste with a $CaO/SiO_2 = 1.13$ (Ecocem) at w/s = 0.50 (light blue) and 0.66 (blue).

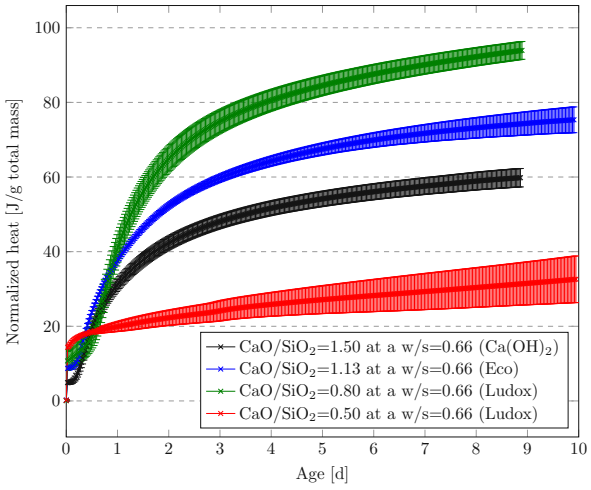

(b) AAS paste with different CaO/SiO_2 at w/s = 0.66.

Fig. 3.7: Normalized accumulated heat of hydration (per gram of total AAS paste weight) as a function of time for AAS pastes with different CaO/SiO_2.

about 08:05 h and for the w/s = 0.66 at about 07:56 h. The peak of the heat of hydration for AAS with a $CaO/SiO_2 = 1.50$ at a w/s = 0.66 occurs at about 08:25 h. The peak of the heat of hydration for the AAS with a $CaO/SiO_2 = 0.80$ at a w/s = 0.66 occurs at about 17:25 h. For the AAS with a $CaO/SiO_2 = 0.50$ at a w/s = 0.66 there is no well defined peak in the first 10 days, as already observed in vicat tests where no initial setting point is reached in the first 120 h.

The normalized accumulated heat over time is shown in Figure 3.7 for $CaO/SiO_2 = 1.13$ at w/s = 0.50 and 0.66 (see Figure 3.7a) and for all CaO/SiO_2 at w/s = 0.66 (see Figure 3.7b). The x-axis shows the age of the mixtures in days. The y-axis of the Figure 3.7 shows the normalized accumulated heat per gram of total paste weight over time in Joule per gram. The increasing slope indicates a continuous heat development during the hydration process. If it reaches a plateau, it means that the majority of chemical reactions in the hydration process have been completed. The highest accumulated heat is about 94 J/g, obtained for the CaO/SiO_2 of 0.80. This is followed by the $CaO/SiO_2 = 1.13$ at a w/s of 0.50 with 53 J/g. The $CaO/SiO_2 = 1.13$ at a w/s of 0.66 reaches a value of about 75 J/g. The CaO/SiO_2 of 1.50 at a w/s of 0.66 reaches about 60 J/g. The lowest accumulated heat, 32 J/g, is achieved by the CaO/SiO_2 of 0.50.

Figure 3.8 shows a comparison of heat of hydration and vicat setting intervals for all AAS formulations. For AAS pastes with $CaO/SiO_2 = 1.13$ at w/s = 0.50 and 0.66, the main hydration peak is located in between the beginning and end of setting as measured by vicat.

It can be seen that a lower w/s leads to a more intense reaction, since the heat flow at w/s = 0.50 is higher than at w/s = 0.66 (see Figure 3.8a), as expected. The peak of the hydration temperature from the isothermal calorimetry experiment of the AAS paste with a CaO/SiO_2 of 1.50 at a w/s of 0.66 occurs at approximately the same time as the initial setting time determined by the vicat tests (see Figure 3.8b). Compared to the AAS paste with a $CaO/SiO_2 = 1.13$ at w/s = 0.66 (reference), the AAS paste with CaO/SiO_2 of 1.50 slightly delays the peak of hydration (about 30 minutes).

The AAS paste with a CaO/SiO_2 of 0.80 at a w/s of 0.66 has a large delay between the initial setting time, determined by the vicat test, and the peak of hydration. An even slower hydration process is visible for AAS pastes with a CaO/SiO_2 of 0.50, where more Ludox (SiO_2) is present. For the $CaO/SiO_2 = 0.50$ at a w/s of 0.66, the initial setting point is not reached

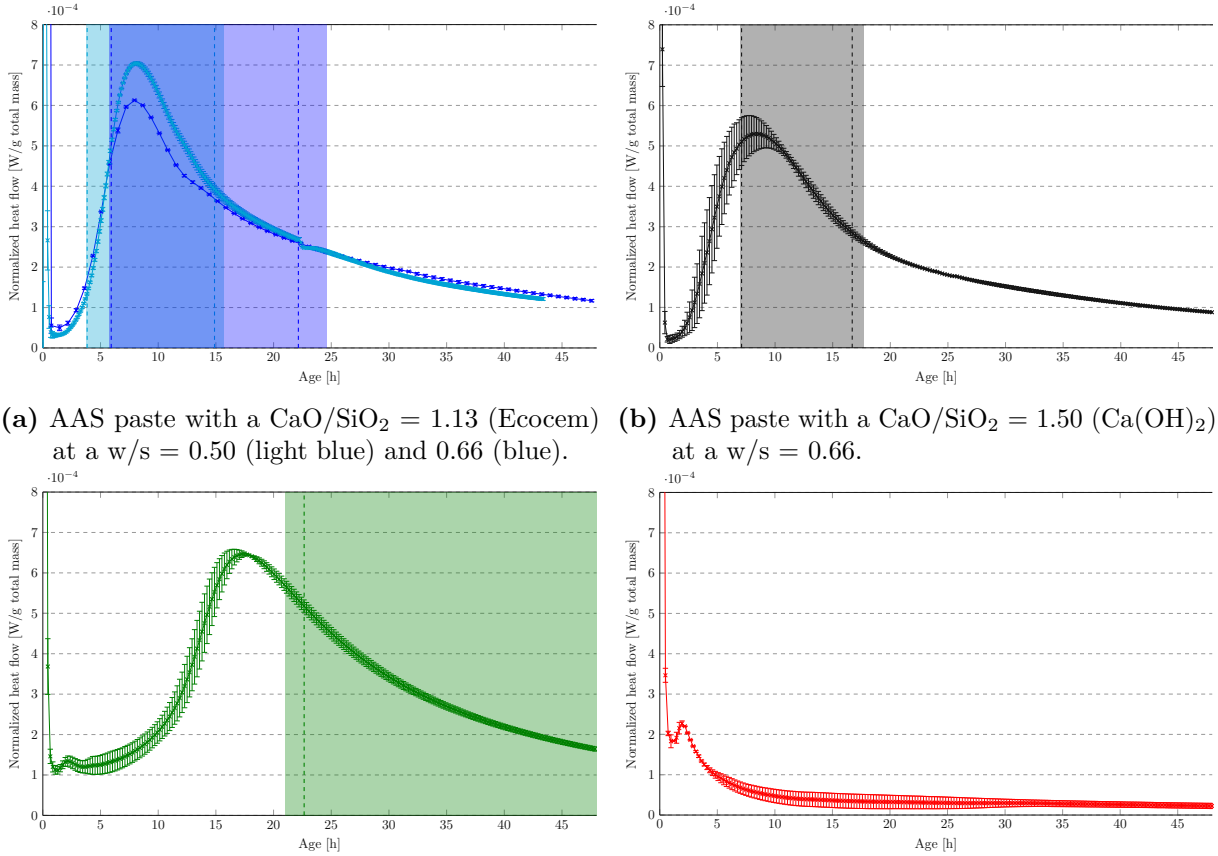

(a) AAS paste with a $CaO/SiO_2 = 1.13$ (Ecocem) at a w/s = 0.50 (light blue) and 0.66 (blue).

(b) AAS paste with a $CaO/SiO_2 = 1.50$ ($Ca(OH)_2$) at a w/s = 0.66.

(c) AAS paste with a $CaO/SiO_2 = 0.80$ (Ludox) at a w/s = 0.66.

(d) AAS paste with a $CaO/SiO_2 = 0.50$ (Ludox) at a w/s = 0.66.

Fig. 3.8: Normalized heat flow (per gram of total AAS paste weight) as a function of time for AAS pastes with different CaO/SiO_2 with a zoom on the first 48 hours of AAS paste aging. The first dashed and colored vertical line indicates the initial setting time, the second the final setting time from vicat tests. The colored area to the left of (t_{start}) or to the right of (t_{end}) shows the error bar (see Table 3.5). The time between the initial and final setting time is also colored.

within a timeframe of 120 hours in the vicat tests. Even the calorimeter results indicate that the hydration does not occur in the time frame studied (10 days).

The peak of heat generation in OPC typically occurs more towards the end of the hardening process [5, 17]. When comparing vicat and calorimetry within AAS formulations, it is challenging to find an exact match between the time of peak occurrence (t_{peak}) and the initial (t_{start}) and final setting times (t_{end}), as shown in Figure 3.9. The isothermal calorimeter provides a more accurate estimation of the hydration process in comparison to the vicat (i.e., more controlled conditions). Moreover the needle penetration in the vicat depends on the granulometric distribution of the paste. The overall heat of hydration of AAS formulations is lower in comparison to OPC. The heat of hydration of OPC is generally 420 J/g. The heat of hydration of CEM III/A 42.5, where 36-65% is slag, is around 300 J/g. The heat of hydration of CEM III/B 32.5, of which 66-80% is slag, is around 210 J/g [14, 36]. The timing in the first hydration peak of OPC is similar to that of AAS pastes with $CaO/SiO_2 = 1.13$ and 1.50. For AAS pastes with lower CaO/SiO_2 the hydration is strongly delayed. Further in situ investigations are needed to delineate the hydration process in AAS formulations.

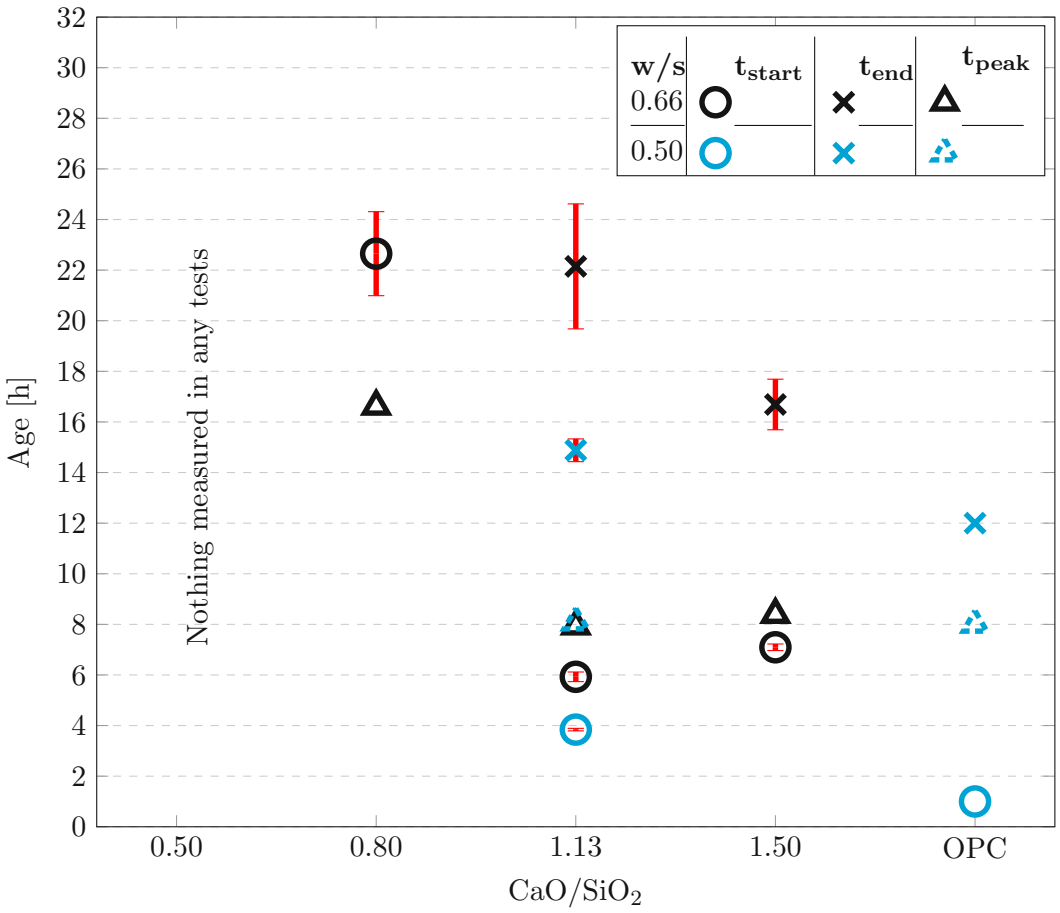

Fig. 3.9: Comparison of initial setting time (t_{start}), peak heat development time t_{peak} and final setting time t_{end} for AAS pastes with different CaO/SiO_2 at w/s = 0.50 (light blue) and 0.66 (black) and OPC [5, 17].

3.5 Mortar prisms tests

The flexural and compressive strengths of AAS mortar prisms are shown in this section. The pastes are mixed with norm sand (see Table 1.2) in a ratio of 1:3 solids (AAS and the solid part from the additives) to sand (see Subsection 2.2.5). Each prism has a dimension of 2 x 2 x 8 cm^3 (see Figure 2.8). The prisms are then stored at room temperature for one day. Then they are demolded and stored in a climate chamber above and under water. The water is saturated with slag (6.0 g/L) to prevent leakage. The AAS mortar prisms with a CaO/SiO_2 = 0.50 and 0.80 are placed under water on the sixth day. For simplicity, the first point is shown on the seventh day. The methodologies are described in section 2.2.5.

3.5.1 Flexural strength R_f

Figure 3.10 illustrates the flexural strength of the AAS mortar prisms with a CaO/SiO_2 = 1.13 at water to solid of 0.50 and 0.66. The x-axis represents the age of each paste in days and the y-axis shows the flexural strength in MPa. The empty circle represents the values of the prisms stored above water, while the filled square represents the values of the prisms stored under water. In the Figure 3.10 it can be seen that for both above and below water storage, higher values are achieved at all times for the w/s 0.50 compared to 0.66 as expected [39]. Figure 3.11 shows

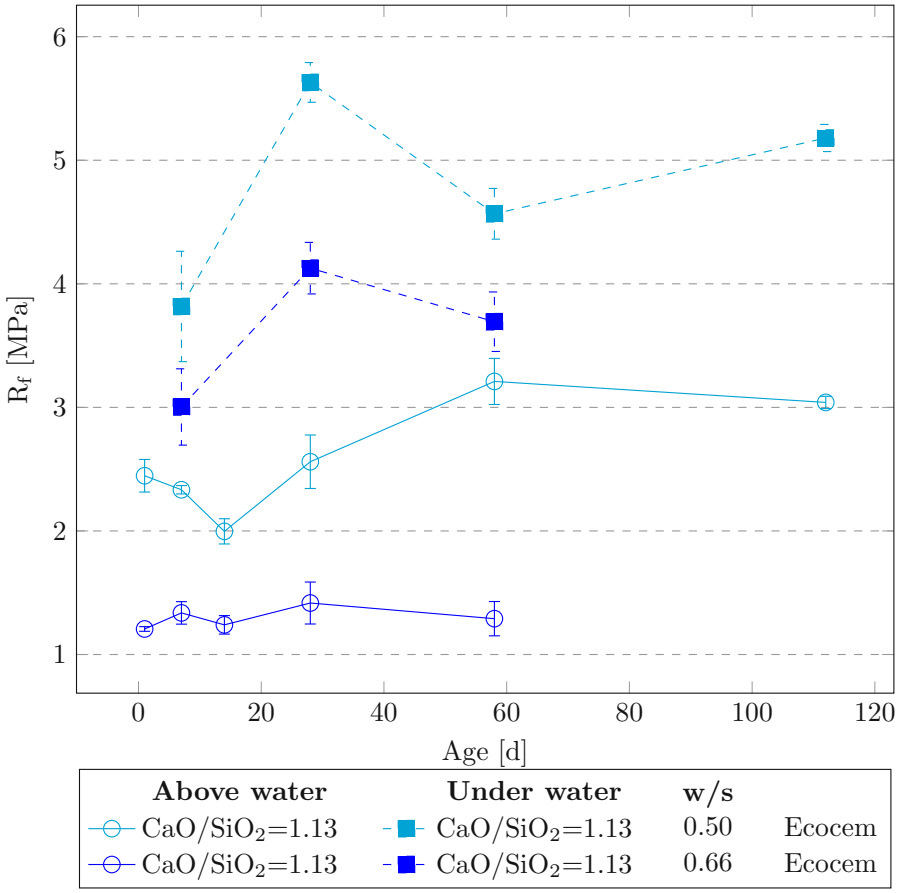

Fig. 3.10: Flexural strength R_f of AAS mortar prisms with a $CaO/SiO_2 = 1.13$ at a w/s = 0.50 and 0.66. The water was saturated with slag to avoid leakage.

the flexural strength of all CaO/SiO_2 mortar prisms at a w/s of 0.66 over 56 days. It can be observed that AAS mortar prisms with $CaO/SiO_2 = 1.13$ and 1.50 have higher values when stored under water. In particular, the underwater flexural strength of AAS mortar prisms with a $CaO/SiO_2 = 1.50$ is slightly higher than that of $CaO/SiO_2 = 1.13$. In contrast, AAS mortar prisms with $CaO/SiO_2 = 0.50$ and 0.80 have higher values when stored above water than when stored under water.

The values for $CaO/SiO_2 = 1.13$ at a w/s of 0.50 above water are higher (3.0 MPa after 112 days) than the ones measured in the master thesis of Pudelko M. [39] for the same formulation (1.3 MPa after 112 days). The values obtained in this study are more similar to the formulation $AAS_{CC}^{1.1,MS}$ from his study (around 3.2 MPa after 112 days). Comparing the values for $CaO/SiO_2 = 1.13$ at a w/s of 0.50 in the underwater storage from this study with those from Pudelko M. [39] in limestone solution, it can be seen that after 112 days the values are similar (respectively 5.2 and 4.7 MPa). His values for the $AAS_{CC}^{1.1,MS}$ formulation (6.8 MPa after 112 days) are higher than the those obtained in this study. Overall from Figure 3.11, it can be seen that the AAS mortar prisms with a $CaO/SiO_2 = 1.13$ and 1.50 have similar flexural strength. The AAS mortar prisms above water with a $CaO/SiO_2 = 0.80$ at a w/s = 0.66 have the fastest increase in flexural strength from day one to day 14 of all the formulations tested in this thesis. Afterwards they reach comparable R_f values (1.6 MPa after 56 days) to the study of Pudelko M. [39] (2.5 MPa after 56 days), even if a lower w/s = 0.50 was used in his study. The AAS mortar prisms below water with a $CaO/SiO_2 = 0.50$ (0.6 MPa after 56 days) and 0.80 (0.7 MPa after 56 days) have

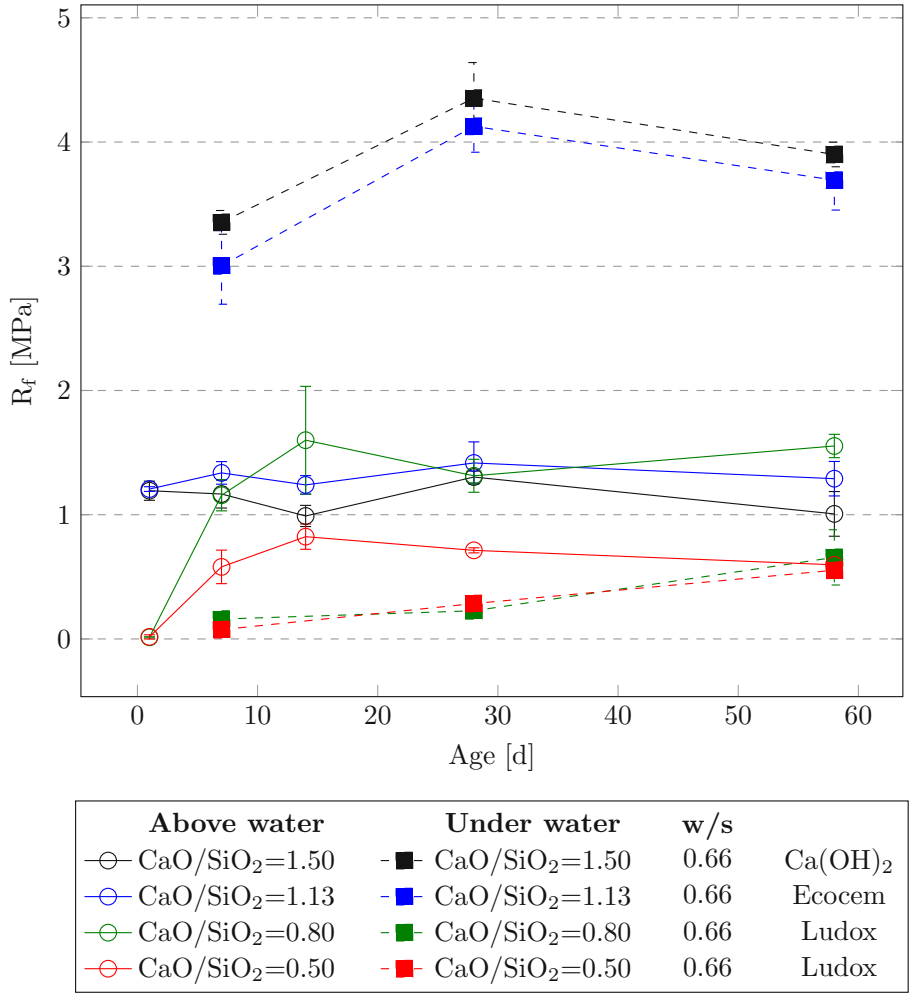

Fig. 3.11: Flexural strength R_f of AAS mortar prisms with for all four CaO/SiO_2 = 0.50, 0.80, 1.13, 1.50 at a w/s = 0.66. The AAS mortar prisms with a CaO/SiO_2 = 0.50 and 0.80 are placed under water on the sixth day. For simplicity, the first point is shown after 7 days. The water was saturated with slag to avoid leakage.

flexural strength values much lower than the results from the AAS mortar prisms with CaO/SiO_2 = 0.80 from Pudelko M. [39] stored in limestone solution (4.7 MPa after 56 days) and with a lower w/s = 0.50.

3.5.2 Compressive strength R_c

Figure 3.12 shows the compressive strength of mortar prisms at a CaO/SiO_2 = 1.13 and w/s 0.50 and 0.66. The x-axis represents the age of each paste in days and the y-axis represents the compressive strength in MPa. The empty circle represents the values of the prisms stored above water, while the filled square represents the values of the prisms stored under water. In the Figure 3.12 it can be seen that for both above and below water storage higher values are achieved at all times for the w/s 0.50 in comparison to the 0.66 as expected [39]. In Figure 3.12, the effect of storage is more visible for AAS mortar prisms at w/s = 0.50, where the compressive strength under water is slightly lower than above water. Figure 3.13 shows R_c for all CaO/SiO_2 mortar prisms at w/s = 0.66 over 56 days. It can be observed that similar values are obtained

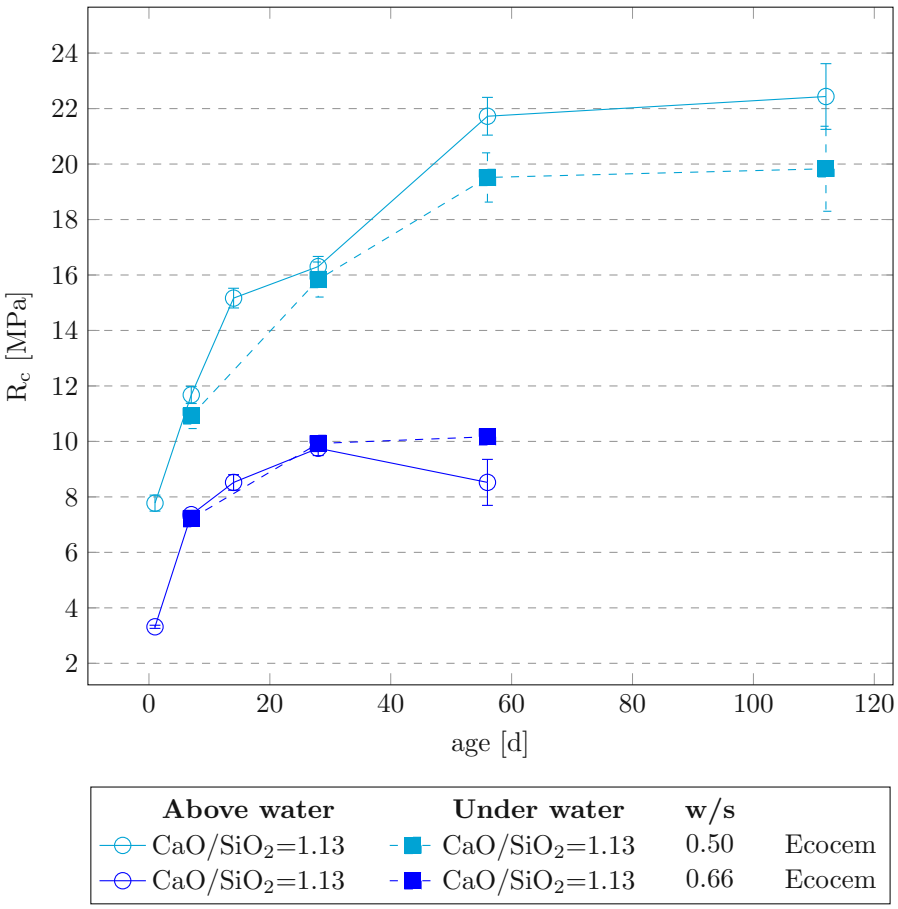

Fig. 3.12: Compressive strength R_c of mortar prisms with a $CaO/SiO_2 = 1.13$ at a w/s = 0.50 and 0.66. The water was saturated with slag to avoid leakage.

for AAS mortar prisms at $CaO/SiO_2 = 1.13$ and 1.50 when stored under and above water. The compressive strength of AAS mortar prisms at a $CaO/SiO_2 = 1.13$ is slightly higher than that of AAS mortar prisms at a $CaO/SiO_2 = 1.50$ when stored under water. In contrast, AAS mortar prisms with $CaO/SiO_2 = 0.50$ and 0.80 have higher values when stored above water than when stored under water. The values for $CaO/SiO_2 = 1.13$ at a w/s of 0.50 above water are higher (22.4 MPa after 112 days) than the ones measured in the master thesis of Pudelko M. [39] for the same formulation (about 12.6 MPa after 112 days). The values obtained in this study are even higher than the formulation $AAS_{CC}^{1.1,MS}$ from his study (about 19.1 MPa after 112 days). Comparing the values for $CaO/SiO_2 = 1.13$ at a w/s of 0.50 in underwater storage from this study (19.8 MPa after 112 days) with those from Pudelko M. [39] in the limestone solution (about 11.4 MPa after 112 days), it can be seen that the values after 112 days in this study are higher. His values for the $AAS_{CC}^{1.1,MS}$ formulation (23.4 MPa after 112 days) are higher than the values achieved in this study.

The AAS mortar prisms above water with a $CaO/SiO_2 = 0.80$ at a w/s = 0.66 have a similar increase in compressive strength as those with a CaO/SiO_2 of 1.13 and 1.50. However, the constant large error bar for AAS mortar prisms at $CaO/SiO_2 = 0.80$ indicates a sensitive formulation. Also the values after 14 days (9.5 MPa) are about 55% less and after 28 days (6.2 MPa) are about one third of the values obtained by Pudelko M. [39] (around 17.0 MPa at day 12 and about 22.6 at day 28) for a $CaO/SiO_2 = 0.80$ above water and stored in the same climatic chamber (w/s = 0.50). The R_c for the AAS mortar prisms with a $CaO/SiO_2 = 0.80$ (1.4 MPa

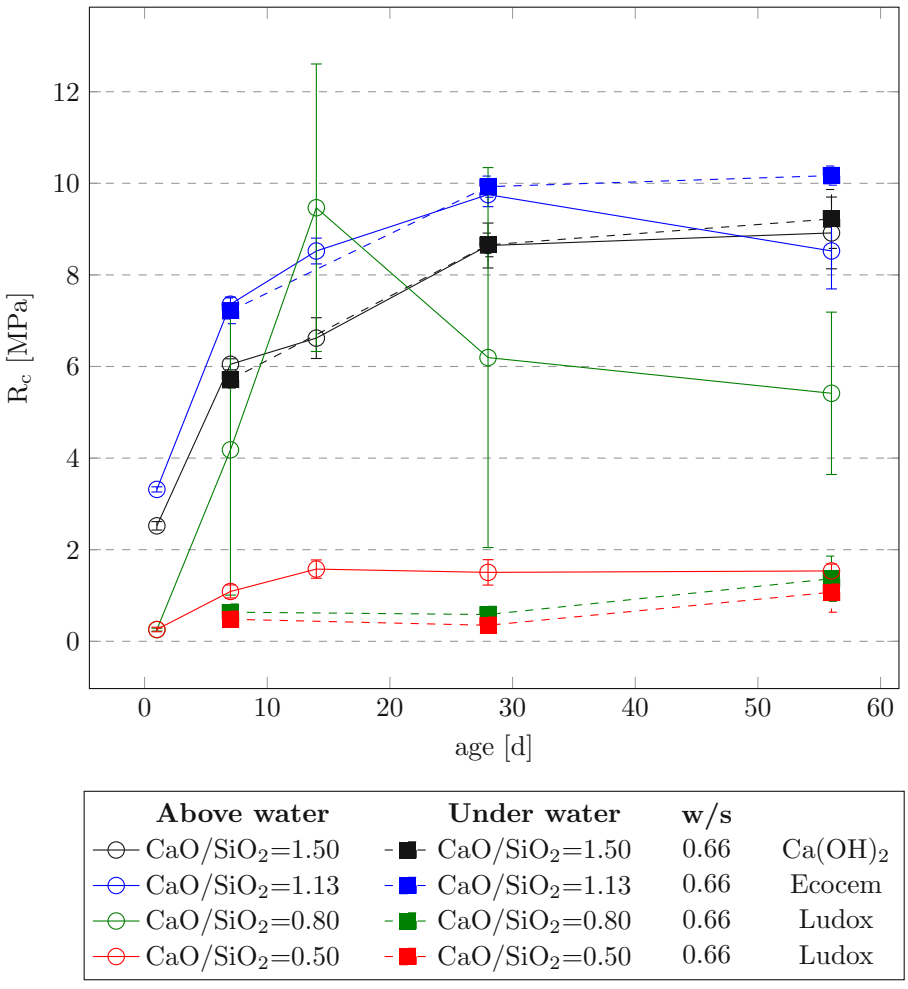

Fig. 3.13: Compressive strength R_c of mortar prisms with for all four CaO/SiO_2 = 0.50, 0.80, 1.13, 1.50 at a w/s = 0.66. The AAS mortar prisms with a CaO/SiO_2 = 0.50 and 0.80 are placed under water on the sixth day. For simplicity, the first point is shown after 7 days. The water was saturated with slag to avoid leakage.

after 56 days) under water storage are even worse compared to Pudelko M. [39] (about 17.8 MPa after 56 days). In his study, the values above water and under a limestone solution are about the same. For the AAS mortar prisms at a CaO/SiO_2 = 0.50, the R_c obtained are the lowest (1.1 MPa after 56 days) of all the formulations tested in this study, as observed for to the flexural strength.

3.6 General discussion

Taking into account all the tests, a general discussion can be made. The AAS formulations containing more SiO_2 show a delay in the hydration process, which is more pronounced when more silica is present. The AAS with CaO/SiO_2 = 0.80 at a w/s = 0.66 shows an increase in mechanical properties after an initial delay. After 14 days for both mechanical test and after 56 days a flexural strength where slightly higher then the reference AAS mortar pastes with CaO/SiO_2 = 1.13 at a w/s = 0.66. However, a large error bar for the mechanical properties from day seven on suggests a very sensitive formulation. Above water, the mechanical properties

after 14 days are about 55% less and after 28 days are about one third of the values obtained by Pudelko M. [39] achieved by AAS mortar prisms with a $CaO/SiO_2 = 0.80$ at a $w/s = 0.50$. In comparison, both mechanical properties for underwater storage are worse than his values obtained for storage in a limestone solution. The AAS at $CaO/SiO_2 = 0.80$ used by Pudelko M. [39] had a different slag source containing different percentages of other oxides (e.g.,MgO). Both AAS mortar prisms with a $CaO/SiO_2 = 0.80$ and 0.50 at a $w/s = 0.66$ do not benefit from underwater storage. The AAS mortar prisms with a $CaO/SiO_2 = 0.50$ show the worst hydration evolution and mechanical properties. It can be said that a lower CaO/SiO_2 is associated with poorer strength values. A higher CaO/SiO_2 is associated with higher mechanical strength values. The AAS mortar prisms with a $CaO/SiO_2 = 1.13$ achieve the highest values for most of the mechanical tests. Except for the flexural strength under water where the AAS mortar prisms with a $CaO/SiO_2 = 1.50$ are always higher. The values of mechanical properties of AAS mortar prisms with a $CaO/SiO_2 = 1.13$ at a w/s 0.50 in this study are higher than the values found in the master's thesis of Pudelko M. [39] for the same formulation. Comparing the AAS mortar prisms with a $CaO/SiO_2 = 1.13$ and 1.50 at $w/s = 0.66$ with the results for AAS mortar with a $CaO/SiO_2 = 1.13$ at a w/s of 0.50 from Pudelko M. [39], the mechanical properties from storage above water are almost the same. This is also true for those stored under water in this study compared to the storage in a limestone solution of Pudelko M. [39]. We can conclude that the AAS samples with more calcium ($CaO/SiO_2 = 1.13$ and 1.50) have a more cement-like behavior in terms of hydration time and mechanical properties evolution. The result obtained in terms of flexural and compressive strength seems to benefit from underwater storage.

Chapter 4

Conclusion and perspectives

This chapter presents the conclusion and perspectives of this work.

The **motivation** for this thesis is the need to replace ordinary Portland cement (OPC), which is responsible for 5 - 8% of total anthropogenic CO_2 emissions [1, 13, 20, 57]. This study focuses on an alkali activated slag (AAS) formulation in which OPC is completely replaced. Two previous studies on similar AAS formulations were made by Aschauer C. [2] and Pudelko M. [39] at TU Wien. In particular, Pudelko M. [39], has shown that different mechanical properties are obtained for different slag sources with different CaO/SiO_2. In the literature the influence of CaO/SiO_2 on the early and long term properties of alkali activated slag is not clear. For this reason, this work focuses on a more systematic approach to vary the CaO/SiO_2 on the same slag source by using additives.

The main precursor is a ground granulated blast slag (GGBS) from Ecocem. The activators used to obtain our AAS are sodium carbonate (Na_2CO_2) and calcium hydroxide ($Ca(OH)_2$). Ecocem has a CaO/SiO_2 of 1.13. Ludox colloidal silica suspension (SiO_2) is used to reduce the CaO/SiO_2 to 0.80 and 0.50, while calcium hydroxide, is also used to increase the CaO/SiO_2 to 1.50. To determine the effect of CaO/SiO_2 in AAS samples, spread, vicat, isothermal calorimetry and mechanical tests were performed for all four CaO/SiO_2 (0.50, 0.80, 1.13 and 1.50) at a w/s = 0.66. In addition the AAS paste with a CaO/SiO_2 = 1.13 is tested at w/s 0.50 (following ÖNORM EN 196-1[33]). In this thesis, we investigate **how variations in CaO/SiO_2, achieved through the use of additives, influence the early and long-term properties of alkali-activated slag (AAS) using the same source of slag throughout all experiments.**

Increasing the CaO/SiO_2 of AAS pastes to 1.50 reduces workability, slightly delays setting, and slightly reduces mechanical properties except flexural strength under water in comparison with a CaO/SiO_2 = 1.13. Lowering the CaO/SiO_2 of AAS pastes to 0.80 and 0.50 using Ludox at the same w/s decreases workability, especially with increased SiO_2 content. The hydration delays significantly spacially when more SiO_2 is present. Mechanical properties are unstable, for CaO/SiO_2 = 0.80 above water. Underwater storage has no benefits, with the worst performance for CaO/SiO_2 = 0.50.

Overall, it can be seen that AAS pastes with more calcium content (CaO/SiO_2 = 1.13 and 1.50) have a more cement-like behavior in terms of hydration and mechanical properties and benefit from storage under water.The AAS pastes with a lower calcium content (CaO/SiO_2 = 0.50 and 0.80) have a drastic delay in the hydration process, which is stronger when more SiO_2 is available. All data of the AAS pastes with CaO/SiO_2 = 0.80 are characterized by a large error bar, suggesting a sensitive formulation. The AAS pastes with CaO/SiO_2 = 0.50 have no setting in 120 hours and have the worst mechanical properties.

As the results show, different CaO/SiO_2 has a great influence on the early and long term properties of the alkali activated slag. Moreover, additives not only change the CaO/SiO_2 of AAS pastes, they also have a strong impact on the initial spread of these pastes due to the key role of specific surface area on water demand. Further studies should focus on more in situ physico-chemical measurements (SEM, NMR, XRD...) to get a better understanding of the

different hydration processes and products. The role of other chemical oxides composing the slag should also be further investigated (MgO, Al_2O_3). Further research should be conducted to quantify the CO_2 emission of the specific AAS formulation from extraction, processing, and final use on the construction site, which would help in the use of AAS as a fully sustainable replacement for OPC.

Chapter 5

Appendix

5.1 Spread test over time for the different batches

As discussed in Subsection 2.2.1, a spread test over time was performed for the three different AAS batches (see Table 5.1) used in this study as well as for the batch used by Pudelko M. [39]. The formulations for the AAS pastes with $CaO/SiO_2 = 1.13$ at a w/s = 0.50 used for the spread over time tests are shown in Table 2.5. Therefore, a mini-cone (see Figure 5.1) was used to test if the different batches of Ecocem have the same spread. The mini-cone is a 40% reduced version of the cone of the European guideline (see Figure 2.2b) [4]. The method of the cone spread test

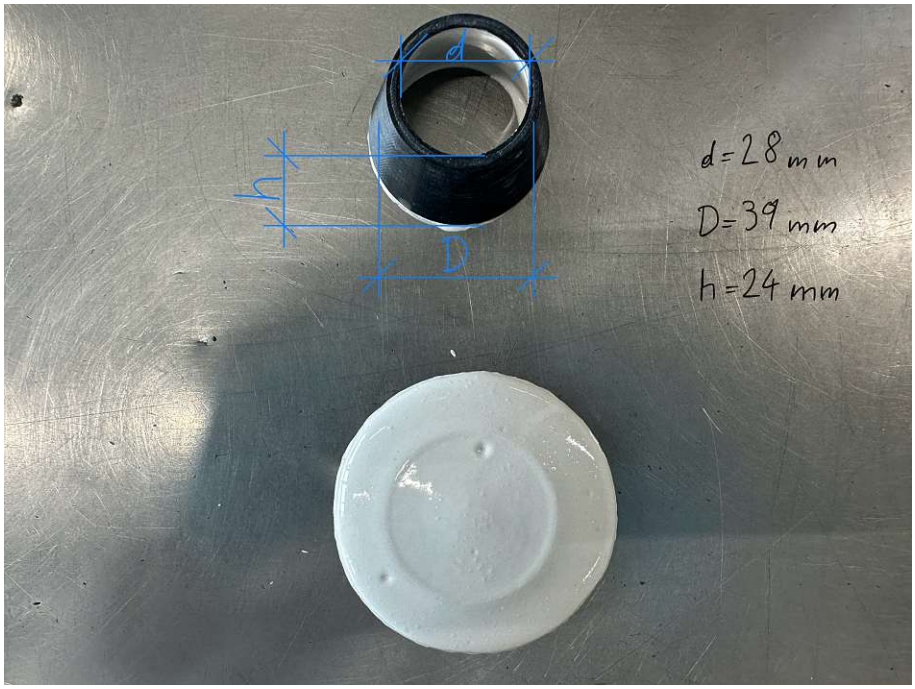

Fig. 5.1: Mini cone for the spread tests over time.

is described in Subsection 2.2.1. In order to prevent evaporation, the mixtures are kept covered between each spread test. Before testing each paste was mixed at 1000 rpm for 1 minute. The exact time when a spread test was performed is shown in Table 5.1. Figure 5.2 shows the spread of the different batches over time. The x-axis shows the age of the mixtures in minutes. The y-axis shows the spread of the mixtures in centimeters. It can be seen that the three batches used in this study have about the same spread after half an hour. The range of variation is about 3.0 mm. This small variation indicates that all three batches used have the same properties. Only the old one used by Pudelko M. [39], which was opened one year ago, has a lower spread

Tab. 5.1: Spread tests at various times and different batches.

CaO/SiO_2	w/s	Batch	Fresh	10'	20'	30'	40'	50'	60'
1.13	0.50	1	x	x	x	x	x	x	x
1.13	0.50	2	x	x		x			x
1.13	0.50	3	x	x		x			x
1.13	0.50	Pudelko M. [39]	x			x			x

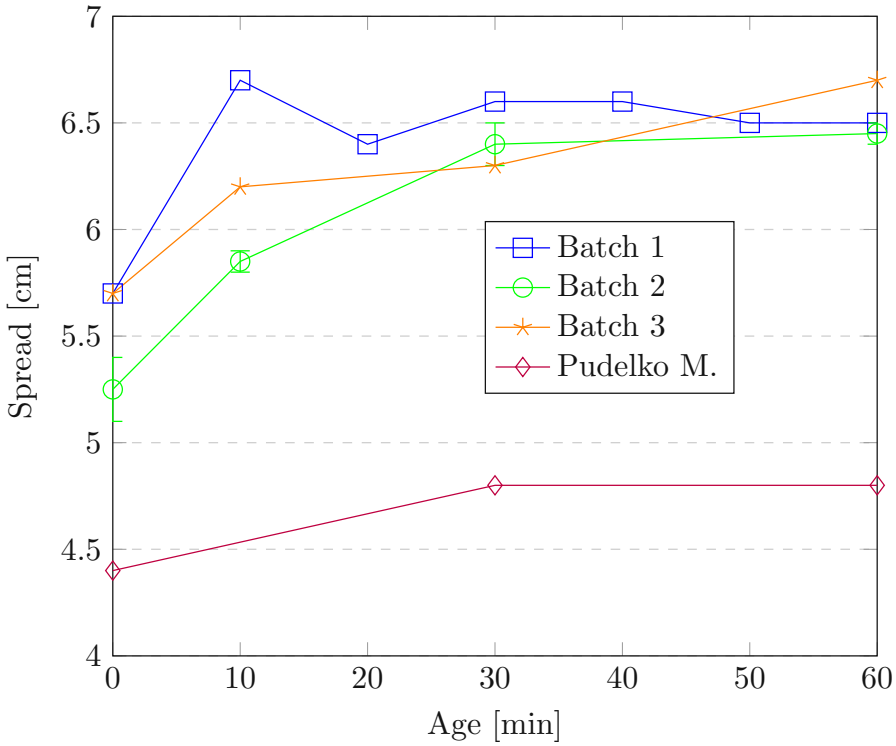

Fig. 5.2: Spread over time for different AAS batches. Batch 1, 2 and the one used by Pudelko MM. [39] are tested on 28.09.2023. Batch 2 is tested a second time on the 06.03.2024 and batch 3 is tested on the 02.10.2023.

over time. This indicates that the properties of the AAS change over time after the batches are opened, as expected.

5.2 Mortar prisms

In addition to the CaO/SiO_2 of 1.50, 1.13, 0.80 and 0.50 at a w/s = 0.66 and CaO/SiO_2 of 1.13 at a w/s = 0.50 carried out in the thesis, some prisms with different CaO/SiO_2 and at different w/s were tested, as follows:

- CaO/SiO_2 = 1.45 at a w/s = 0.66 and 0.44
- CaO/SiO_2 = 0.83 at a w/s = 0.50 and 0.45
- CaO/SiO_2 = 0.60 at a w/s = 0.51 and 0.39

The methods are identical to those described in Section 2.2.5. The results are shown in Figure 5.3 and 5.4. The x-axis shows the cringing time in days. The y-axis shows the flexural and compressive strength in MPa. The trend of worse technical values for AAS mortar prisms with a low is confirmed. The AAS mortar prisms with $CaO/SiO_2 = 0.60$ at different w/s (0.39 and 0.45) also reach noteworthy values. The trend that underwater storage has a positive effect on the low CaO/SiO_2 AAS mortar prisms from day 28 onward is also confirmed. Furthermore, it can be seen that at a high $CaO/SiO_2 = 1.45$ in the AAS mortar prisms, the reduction of the w/s to 0.44 has a small positive effect, except for the values of the flexural strength above water after 112 days. In contrast to the AAS mortar prisms with $CaO/SiO_2 = 0.80$, the reduction of the w/s ratio to 0.50 and 0.45 provides significant benefits. Their flexural and compressive strength values are the highest for both above and below water conditions, except for the flexural strength above water at 112 days.

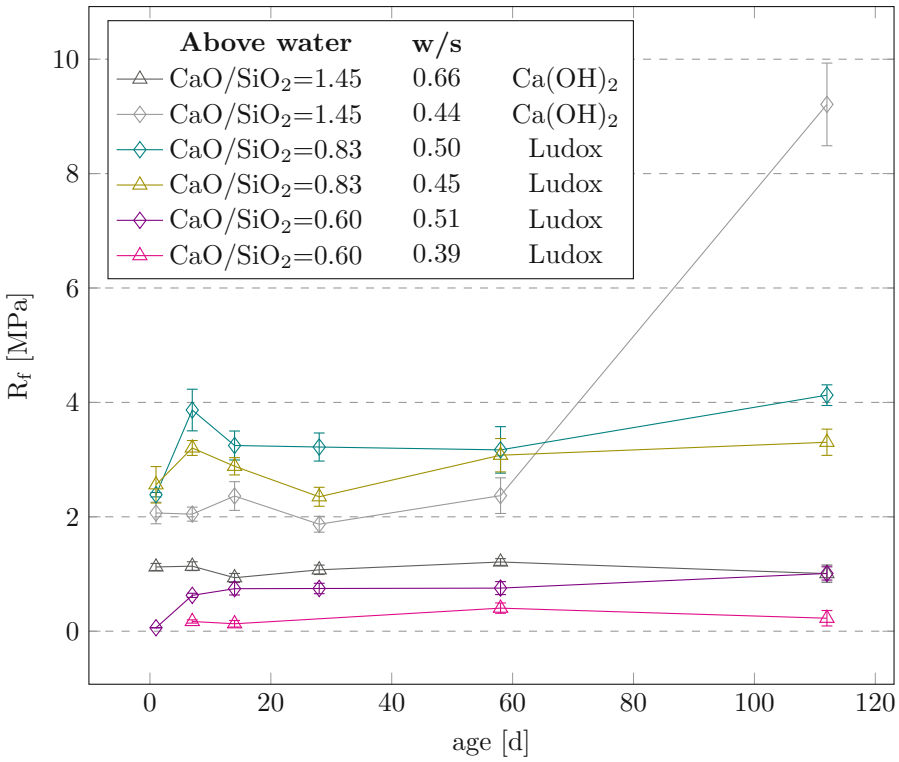

(a) Flexural strength R_f of AAS mortar prisms with different CaO/SiO_2 and different w/s above and water.

Fig. 5.3: Flexural strength R_f of AAS mortar prisms with different CaO/SiO_2 and different w/s **(a)** above and **(b)** under water.

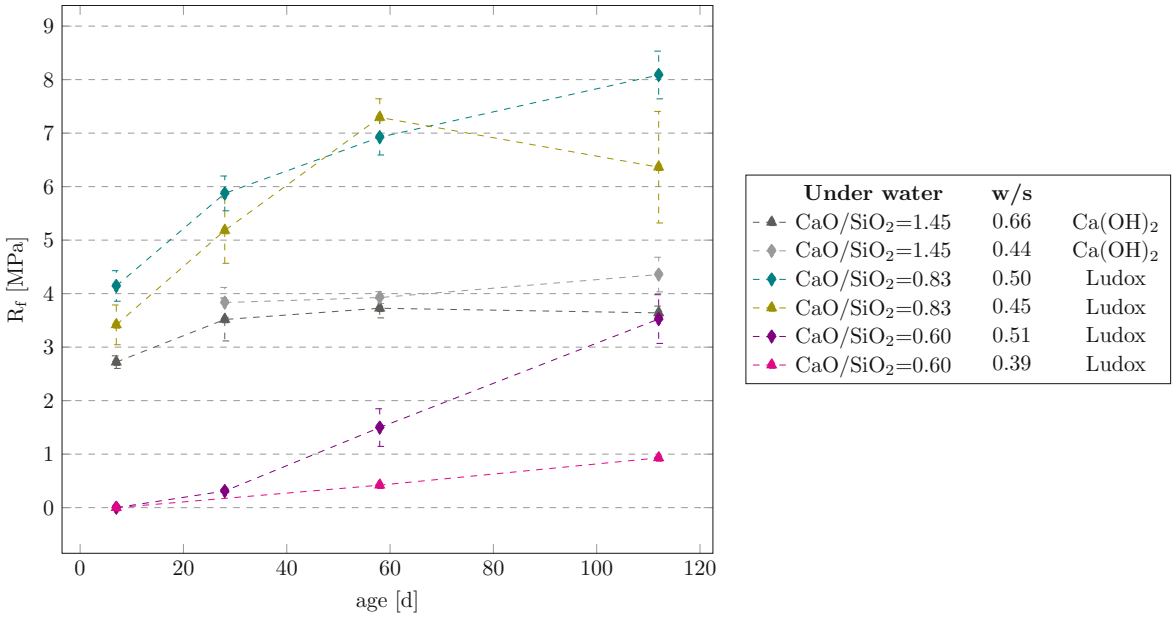

(b) Flexural strength R_f of AAS mortar prisms with different CaO/SiO_2 and different w/s under and water.

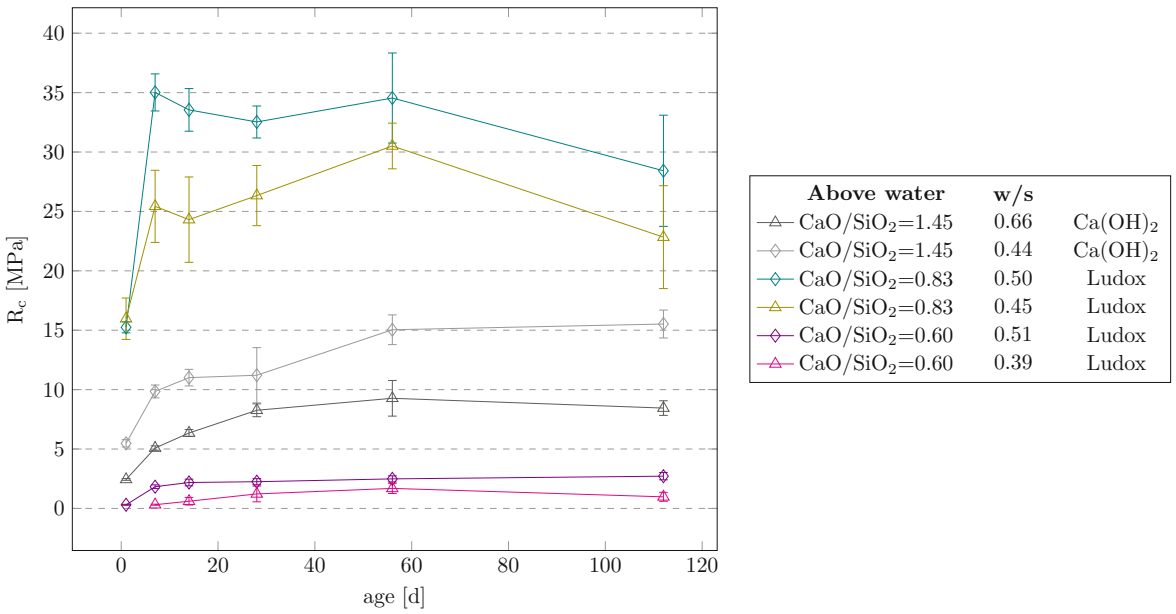

(a) Compressive strength R_c of AAS mortar prisms with different CaO/SiO_2 and different w/s above water.

Fig. 5.4: Compressive strength R_c of AAS mortar prisms with different CaO/SiO_2 and different w/s **(a)** above and **(b)** under water.

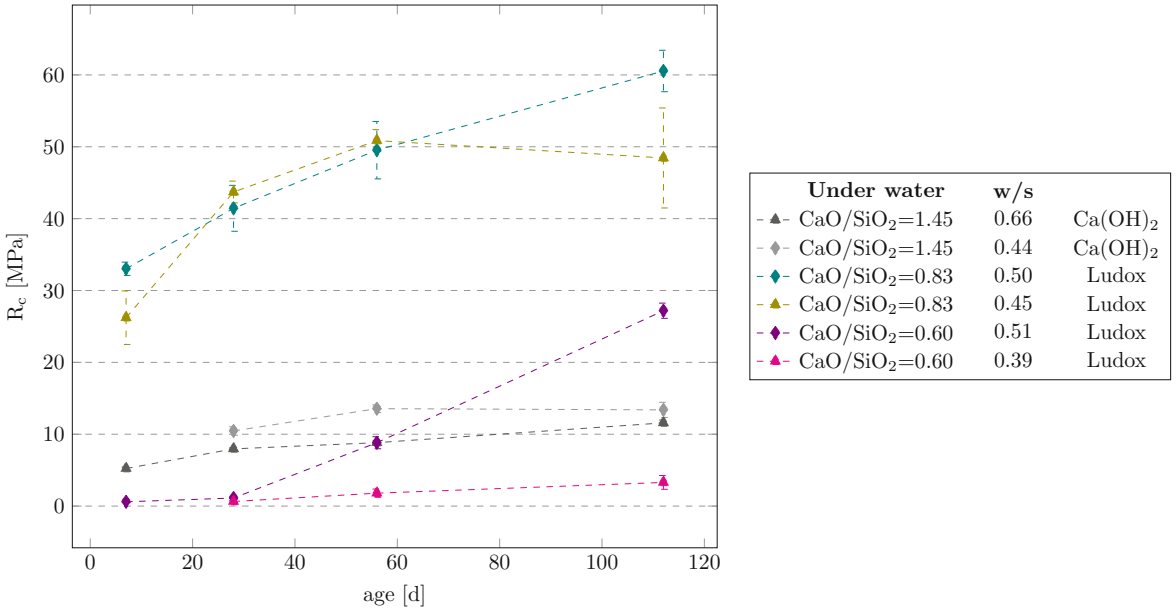

(b) Compressive strength R_c of AAS mortar prisms with different CaO/SiO_2 and different w/s under water.

Bibliography

[1] R. M. Andrew. "Global CO2 emissions from cement production, 1928-2018". eng. In: *Earth system science data* 11.4 (2019), pp. 1675–1710. ISSN: 1866-3508.

[2] C. Aschauer. *Untersuchung der Frisch- und Festigkeitseigenschaften von nachhaltigem Zement (AAB)*. ger. Wien, 2022.

[3] J. Beaudoin and I. Odler. "5 - Hydration, Setting and Hardening of Portland Cement". In: *Lea's Chemistry of Cement and Concrete (Fifth Edition)*. Ed. by P. C. Hewlett and M. Liska. Fifth Edition. Butterworth-Heinemann, 2019, pp. 157–250. ISBN: 978-0-08-100773-0. DOI: https://doi.org/10.1016/B978-0-08-100773-0.00005-8. URL: https://www.sciencedirect.com/science/article/pii/B9780081007730000058.

[4] bibm, CEMBUREAU; EFCA; EFNARC; ERMCO. *Europäische Richtlinien für SCC Homepage*. 2005. URL: https://www.gvtb.at/docs/technische-unterlagen/SSC_Richtlinien.pdf (Zugriff am 04/17/2024).

[5] E. Bölcskey and H. Bruckner. *Bindemittel*. ger. Wien, 2014.

[6] E. Bölcskey and H. Bruckner. *Frischbeton*. ger. Wien, 2014.

[7] Chemlab analytical. *Chemlab Homepage*. 2024. URL: https://www.chemlab-analytical.be/#/en-gb (Zugriff am 03/22/2024).

[8] Chemlab analytical. *Merck Homepage*. 2024. URL: https://www.sigmaaldrich.com/AT/de/product/aldrich/420778 (Zugriff am 03/22/2024).

[9] CRYSTRAN. *CRYSTRAN ALWAYS ON YOUR WAVELENGTH*. 2024. URL: https://www.crystran.co.uk/optical-materials/magnesium-oxide-mgo (Zugriff am 04/13/2024).

[10] Ecocem. *Ecocem Homepage*. 2024. URL: https://www.ecocemglobal.com/ (Zugriff am 03/12/2024).

[11] Q. Fu, M. Bu, Z. Zhang, W. Xu, Q. Yuan, and D. Niu. "Hydration Characteristics and Microstructure of Alkali-Activated Slag Concrete: A Review". In: *Engineering* 20 (2023), pp. 162–179. ISSN: 2095-8099. DOI: https://doi.org/10.1016/j.eng.2021.07.026. URL: https://www.sciencedirect.com/science/article/pii/S2095809921005221.

[12] Q. Fu, M. Bu, Z. Zhang, W. Xu, Q. Yuan, and D. Niu. "Hydration Characteristics and Microstructure of Alkali-Activated Slag Concrete: A Review". eng. In: *Engineering (Beijing, China)* 20.1 (2023), pp. 162–179. ISSN: 2095-8099.

[13] I. Garcia-Lodeiro, A. Palomo, and A. Fernández-Jiménez. "An overview of the chemistry of alkali-activated cement-based binders". eng. In: *Handbook of Alkali-Activated Cements, Mortars and Concretes*. 2015, pp. 19–47. ISBN: 1782422765.

[14] E. Gartner, J. Young, D. Damidot, and I. Jawed. "Hydration of Portland cement". In: *Structure and performance of cements* 2 (2002), pp. 57–113.

[15] IMF. *IWF Prognose: Wachstum des realen Bruttoinlandsprodukts (BIP) in den wichtigsten Industrie- und Schwellenländern in den Jahren 2022 bis 2025*. gegenüber dem Vorjahr [Graph]. Statista. Jan. 30, 2024. URL: https://de.statista.com/statistik/daten/studie/38043/umfrage/prognose-zur-entwicklung-des-bip-in-ausgewaehlten-laendern/ (Zugriff am 04/26/2024).

[16] Internetchemie.info. *Internetchemie.info ChemLin Die naturwissensachftliche Wissensdatenbank*. 2024. URL: https://www.internetchemie.info/substanz/Natriumcarbonat.php (Zugriff am 04/13/2024).

[17] D. Jansen, F. Goetz-Neunhoeffer, B. Lothenbach, and J. Neubauer. "The early hydration of Ordinary Portland Cement (OPC): An approach comparing measured heat flow with calculated heat flow from QXRD". eng. In: *Cement and concrete research* 42.1 (2012), pp. 134–138. ISSN: 0008-8846.

[18] D. Jiang, C. Shi, and Z. Zhang. "Recent progress in understanding setting and hardening of alkali-activated slag (AAS) materials". In: *Cement and Concrete Composites* 134 (2022), p. 104795. ISSN: 0958-9465. DOI: https://doi.org/10.1016/j.cemconcomp.2022.104795. URL: https://www.sciencedirect.com/science/article/pii/S0958946522003882.

[19] Korth Kristalle GmbH. *KORTH KRISTALLLE*. 2024. URL: https://www.korth.de/material/detail/Quarz,%20kristallin (Zugriff am 04/13/2024).

[20] X. Li, H. Grassl, C. Hesse, and J. Dengler. "Unlocking the potential of ordinary Portland cement with hydration control additive enabling low-carbon building materials". eng. In: *Communications materials* 5.1 (2024), pp. 1–9. ISSN: 2662-4443.

[21] T. Liberto, M. Bellotto, and A. Robisson. "Small oscillatory rheology and cementitious particle interactions". In: *Cement and Concrete Research* 157 (2022), p. 106790. ISSN: 0008-8846. DOI: https://doi.org/10.1016/j.cemconres.2022.106790. URL: https://www.sciencedirect.com/science/article/pii/S0008884622000813.

[22] T. Liberto, M. C. Dalconi, G. Dal Sasso, M. Bellotto, and A. Robisson. "Structure–function relationship during the early and long-term hydration of one-part alkali-activated slag". eng. In: *Journal of the American Ceramic Society* 106.9 (2023), pp. 5187–5202. ISSN: 0002-7820.

[23] B. Lothenbach and A. Nonat. "Calcium silicate hydrates: Solid and liquid phase composition". In: *Cement and Concrete Research* 78 (2015). Keynote papers from 14th International Congress on the Chemistry of Cement (ICCC 2015), pp. 57–70. ISSN: 0008-8846. DOI: https://doi.org/10.1016/j.cemconres.2015.03.019. URL: https://www.sciencedirect.com/science/article/pii/S0008884615001052.

[24] X. Luo and C. a. Wang. "Effect of calcia content on structure and properties of metakaolin/blast furnace slag-based geopolymers". In: *J. Chin. Ceram. Soc* 43 (2015), pp. 1800–1805.

[25] MatWeb. *MatWeb Material Property Data*. 2024. URL: https://www.matweb.com/search/datasheet.aspx?matguid=204094cb0fd34c099b8a52c9c7df1d5c&ckck=1 (Zugriff am 04/13/2024).

[26] NIST Chemistry. *NIST Chemistry WebBook, SRD 69*. 2024. URL: https://webbook.nist.gov/cgi/cbook.cgi?ID=C7446119&Units=SI&Mask=1&Type=JANAFG&Plot=on#JANAFG (Zugriff am 04/13/2024).

[27] H. Okamura. "Self-compacting high-performance concrete". eng. In: *Concrete international* 19.7 (1997), pp. 50–54. ISSN: 0162-4075.

[28] H. Okamura, K. Maekawa, and K. Ozawa. “DEVELOPMENT OF SELF-COMPACTING HIGH PERFORMANCE CONCRETE”. eng. In: *Doboku Gakkai Ronbunshu* 1995.522 (1995), pp. 23–26. ISSN: 0289-7806.

[29] H. Okamura and M. Ouchi. “Self-Compacting Concrete”. eng. In: *Journal of Advanced Concrete Technology* 1.1 (2003), pp. 5–15. ISSN: 1346-8014.

[30] *ÖNORM B 4710-1:2018 01:Beton — Festlegung, Eigenschaften, Herstellung, Verwendung und Konformität - Teil 1: Regeln zur Umsetzung der ÖNORM EN 206 für Normal- und Schwerbeton*. Deutsch. Wien: Austrian Standards, Jan. 2018.

[31] *ÖNORM EN 12350-5:2019 08 15: Testing fresh concrete - part 5: Flow table test*. English. Wien: Austrian Standards, Aug. 2019.

[32] *ÖNORM EN 12350-5:2019 11 15: Testing fresh concrete - part 1: Sampling and common apparatus*. English. Wien: Austrian Standards, Nov. 2019.

[33] *ÖNORM EN 196-1:2016 10 15: Methods of testing cement - part 1: Determination of strength*. English. Wien: Austrian Standards, Oct. 2016.

[34] *ÖNORM EN 196-11:2019 02 15: Methods of testing cement - part 11: Heat of hydration - Isothermal Conduction Calorimetry method*. English. Wien: Austrian Standards, Jan. 2017.

[35] *ÖNORM EN 196-3:2017 01 01: Methods of testing cement - part 3: Determination of setting times and soundness*. English. Wien: Austrian Standards, Jan. 2017.

[36] *ÖNORM EN 197-1:2016 10 15: Cement - part 1: Composition, specifications and conformity criteria for common cements*. English. Wien: Austrian Standards, Oct. 2011.

[37] *ÖNORM EN 197-5:2021 06 15: Cement - part 5: Portland- composite cement CEM II/C-M and Composite cement CEM VI*. English. Wien: Austrian Standards, June 2021.

[38] *Prüfverfahren Beton (PVB) Nationale Anwendung der Prüfnormen für Beton und seiner Ausgangsstoffe = Test methods for concrete — National application of testing standards for concrete and its source materials*. ger. Ausg.: 2010-09-01. ON-Regel 23303. Wien: Österr. Normungsinst., 2010.

[39] M. Pudelko. *Durability of slag-based alkali activated binder (AAB) = Dauerhaftigkeit von schlackenbasierten, alkalisch aktivierten Bindemitteln (AAB)*. eng. Wien, 2023.

[40] J. Rahou, H. Rezqi, M. El Ouahabi, and N. Fagel. “Characterization of Moroccan steel slag waste: The potential green resource for ceramic production”. eng. In: *Construction and building materials* 314 (2022), p. 125663. ISSN: 0950-0618.

[41] René Rausch. *Das Periodensystem der Elemente online Calciumhydroxid, Ca(OH)2*. 2024. URL: `https://www.periodensystem-online.de/index.php?el=20&id=compound&cpid=1025` (Zugriff am 04/13/2024).

[42] René Rausch. *Das Periodensystem der Elemente online Calciumoxid, CaO*. 2024. URL: `https://www.periodensystem-online.de/index.php?el=20&id=compound&cpid=157` (Zugriff am 04/13/2024).

[43] René Rausch. *Das Periodensystem der Elemente online Eisen(III)oxid, Fe2O3*. 2024. URL: `https://www.periodensystem-online.de/index.php?el=26&id=compound&cpid=334` (Zugriff am 04/13/2024).

[44] René Rausch. *Das Periodensystem der Elemente online Kaliumoxid, K2O*. 2024. URL: `https://www.periodensystem-online.de/index.php?el=19&id=compound&cpid=20` (Zugriff am 04/13/2024).

[45] René Rausch. *Das Periodensystem der Elemente online Mangan(II)oxid, MnO*. 2024. URL: https://www.periodensystem-online.de/index.php?el=25&id=compound&cpid=460 (Zugriff am 04/13/2024).

[46] René Rausch. *Das Periodensystem der Elemente online Natriumoxid, Na2O*. 2024. URL: https://www.periodensystem-online.de/index.php?el=11&id=compound&cpid=13 (Zugriff am 04/13/2024).

[47] René Rausch. *Das Periodensystem der Elemente online Titan(IV)oxid, TiO2*. 2024. URL: https://www.periodensystem-online.de/index.php?el=8&id=compound&cpid=505 (Zugriff am 04/13/2024).

[48] N. Roussel and P. Coussot. ""Fifty-cent rheometer" for yield stress measurements: From slump to spreading flow". eng. In: *Journal of rheology (New York : 1978)* 49.3 (2005), pp. 705–718. ISSN: 0148-6055.

[49] "So wird Beton umweltfreundlich". ger ; eng. In: *Beton- und Stahlbetonbau* 111.10 (2016), pp. 634–634. ISSN: 0005-9900.

[50] Z. Tan, S. A. Bernal, and J. L. Provis. "Reproducible mini-slump test procedure for measuring the yield stress of cementitious pastes". eng. In: *Materials and structures* 50.6 (2017), pp. 235–12. ISSN: 1359-5997.

[51] F. P. Torgal. *Handbook of alkali-activated cements, mortars and concretes*. eng. 1st ed. Woodhead Publishing Series in Civil and Structural Engineering ; Cambridge, England: Elsevier : Woodhead Publishing, 2015. ISBN: 1782422889.

[52] US Geological Survey. *Produktion von Zement nach den wichtigsten Ländern weltweit im Jahr 2023*. In Millionen Tonnen [Graph]. Statista. Jan. 31, 2024. URL: https://de.statista.com/statistik/daten/studie/153695/umfrage/produktion-von-zement-nach-laendern/ (Zugriff am 04/26/2024).

[53] US Geological Survey. *Weltweite Produktion von Zement im Zeitraum von 1995 bis 2023 (in Milliarden Tonnen) [Graph]*. German. Accessed April 25, 2024. Jan. 2024. URL: https://de.statista.com/statistik/daten/studie/1320914/umfrage/weltweite-produktion-von-zement/ (Zugriff am 04/25/2024).

[54] Verein Deutscher Zementwerke e.V. *Zement-Taschenbuch. 51. Auflage*. 51st ed. Erkrath: Verein Deutscher Zementwerke e.V., June 2008, p. 912. ISBN: 978-3-7640-0499-6.

[55] X. Wang, C. Li, G. Chen, H. Lin, W. Wu, Q. Wang, and Q. Lan. "Effect of CaO/SiO2 and Al2O3/SiO2 on the chloride permeability of one-part alkali-activated nickel slag concrete". In: *Construction and Building Materials* 411 (2024), p. 134348. ISSN: 0950-0618. DOI: https://doi.org/10.1016/j.conbuildmat.2023.134348. URL: https://www.sciencedirect.com/science/article/pii/S0950061823040667.

[56] G. Wischers. "Ansteifen und Erstarren von Zement und Beton". In: (1981).

[57] P. Wu, B. Xia, and X. Zhao. "The importance of use and end-of-life phases to the life cycle greenhouse gas (GHG) emissions of concrete – A review". In: *Renewable and Sustainable Energy Reviews* 37 (2014), pp. 360–369. ISSN: 1364-0321. DOI: https://doi.org/10.1016/j.rser.2014.04.070. URL: https://www.sciencedirect.com/science/article/pii/S1364032114003086.

List of Figures

List of Tables